Remote Sensing of Environment 115 (2011) 2986–3001

Contents lists available at ScienceDirect

Remote Sensing of Environment

journal homepage: www.elsevier.com/locate/rse

Ocean transparency from space: Validation of algorithms estimating Secchi depth using MERIS, MODIS and SeaWiFS data

Maéva Doron [a,b,c,*], Marcel Babin [b,c], Odile Hembise [a], Antoine Mangin [a], Philippe Garnesson [a]

[a] ACRI-ST, 260 route du Pin Montard, B.P. 234, 06904 Sophia Antipolis, France
[b] Université Pierre et Marie Curie-Paris 6, Laboratoire d'Océanographie de Villefranche, 06230 Villefranche-sur-Mer, France
[c] CNRS, Laboratoire d'Océanographie de Villefranche, 06230 Villefranche-sur-Mer, France

ARTICLE INFO

Article history:
Received 4 January 2011
Received in revised form 28 April 2011
Accepted 29 May 2011
Available online 12 August 2011

Keywords:
Transparency
Secchi
Visibility
Coastal
Ocean color
Remote-sensing
MERIS
MODIS
SeaWiFS
Semi-analytical algorithm

ABSTRACT

Ocean transparency, often measured using Secchi disk, is a useful index of water quality or productivity and is used in many environmental studies. The spaceborne ocean color sensors provide synoptic and regular radiometric data and can be used for applying environmental policies if the data is converted into relevant biogeochemical properties. We adapted and developed semi-analytical and empirical algorithms to estimate the Secchi depth from satellite ocean color data in both coastal and oceanic waters. The development of the algorithms is based on the use of a comprehensive in situ bio-optical dataset. The algorithms are validated using an extensive set of coincident satellite estimates and in situ measurements of the Secchi depth (so-called matchups). More than 400 matchups are compiled for the MERIS, MODIS and SeaWiFS sensors. The comparison between Secchi depth retrievals from remote sensing data and in situ measurements yields determination coefficients (R^2) between 0.50 and 0.73, depending on the sensor and algorithm. The type II linear regression slopes and intercepts vary between 0.95 and 1.46, and between −0.8 and 6.2 m, respectively. While semi-analytical algorithms provide the most promising results on in situ data, the empirical one proves to be more robust on remote sensing data because it is less sensitive to error due to erroneous atmospheric corrections. Using ocean color archives, one can derive maps of ocean transparency for different areas. Our climatology of the Secchi depth based on ocean color for the transition zone between the North Sea and Baltic Sea is compared to an historical dataset.

1. Introduction

Ocean transparency, although being an apparently vague and generic term, is relevant to many users of marine resources, as an indicator of water quality. The Secchi disk depth (Z_{SD}, in m, see Table 1 for a list of symbols) is a widely used indicator of ocean transparency. This measurement originates from the nineteenth century (see Preisendorfer, 1986; Tyler, 1968 and references therein) and has been routinely made over decades in many areas of the world ocean. Large Secchi depth historical databases therefore exist. The United States National Oceanographic Data Center (US-NODC), for instance, archives ~160 000 observations in the WOD98 dataset (http://www.nodc.noaa.gov/). Historical datasets were used to analyze the temporal trends in the Secchi depth and to associate changes in the transparency with biological components of the oceans or to compute climatologies. Simonot and Le Treut(1986) used that dataset to infer trends in the phytoplanktonic content of the oceans. Another study focused on global patterns of ocean transparency in relation with the new production of the open ocean (Lewis et al., 1988). Falkowski and Wilson(1992) examined the multidecadal variations in the phytoplankton productivity in the North Pacific, estimated from Secchi depth. The latter three studies used the historical measurements of the NODC and took advantage of the link between the Secchi depth and the phytoplanktonic content of the open ocean. Aarup(2002) gathered several thousands of historical observations from the North Sea and the Baltic Sea and derived a climatology for the Skagerrak and Kattegat straits, which link the two seas.

The ocean color spaceborne sensors, thanks to their revisitation capacity and swath width, provide a wealth of information on the ocean and more specifically on substances and processes that interact with, and are driven by light, respectively. Two currently flying sensors, MODIS-Aqua (aboard the Aqua satellite) and MERIS (aboard the Envisat satellite) were launched in 2002 respectively by the NASA and ESA and are expected to provide operational information for some additional years. The SeaWiFS sensor, launched by the NASA provides ocean color data from 1997, which thus constitutes an archive of more than a decade. Although the spatial coverage of ocean color sensors varies with latitude and depends on the cloud coverage, remotely sensed data makes it possible to retrieve not only global views of

* Corresponding author at: Laboratoire des Ecoulements Géophysiques et Industriels, Domaine Universitaire, BP 53, 38041 Grenoble cedex 9, France. Tel.: +33 4 76 82 50 12; fax: +33 4 76 82 52 71.
E-mail address: doron@hmg.inpg.fr (M. Doron).

0034-4257/$ – see front matter © 2011 Elsevier Inc. All rights reserved.
doi:10.1016/j.rse.2011.05.019

Table 1
List of symbols, units and subscripts.

Symbol	Description	Unit
$a(\lambda)$	Absorption coefficient	m^{-1}
$b(\lambda)$	Scattering coefficient	m^{-1}
$b_b(\lambda)$	Backscattering coefficient	m^{-1}
$\tilde{b}_{bp}(\lambda)$	Backscattering efficiency for the particles	Dimensionless
$B_{490-560}$	Average ratio of the scattering coefficient at 490 and 560 nm	Dimensionless
$c(\lambda)$	Beam attenuation coefficient	m^{-1}
$c(v)$	Photopic beam attenuation coefficient	m^{-1}
C_0	Inherent contrast between the disk and background water	Dimensionless
C_{min}	Minimum apparent contrast perceivable by the human eye	Dimensionless
$E_d(\lambda,z)$	Downward plane irradiance at the depth z	$W\,m^{-2}\,nm^{-1}$
$E_u(\lambda,z)$	Upward plane irradiance at the depth z	$W\,m^{-2}\,nm^{-1}$
$f(\lambda)$	Proportionality factor between $R(\lambda)$, $b_b(\lambda)$ and $a(\lambda)$ with $R(\lambda)=f(\lambda)\frac{b_b(\lambda)}{a(\lambda)}$	Dimensionless
$K_d(\lambda)$	Vertical diffuse attenuation coefficient	m^{-1}
$K_d(v)$	Photopic vertical diffuse attenuation coefficient	m^{-1}
$L_u(\lambda,\theta,\varphi,z)$	Upwelling radiance in the viewing direction	$W\,m^{-2}\,sr^{-1}\,nm^{-1}$
$L_w(\lambda,0^+)$	Water-leaving radiance in the viewing direction	$W\,m^{-2}\,sr^{-1}\,nm^{-1}$
n	Refractive index of water	
$nL_u(\lambda,\theta,\varphi,z)$	Normalized water-leaving radiance in the viewing direction	$W\,m^{-2}\,sr^{-1}\,nm^{-1}$
Q	Bidirectionality factor	Dimensionless
$r_{rs}(\lambda)$	In-water remote-sensing reflectance	sr^{-1}
$\bar{r}$	Mean (water–air) Fresnel reflectance for the whole diffuse upward flux	Dimensionless
$R(\lambda)$	Irradiance reflectance just below the surface	Dimensionless
$R_{rs}(\lambda)$	Above-surface remote-sensing reflectance	sr^{-1}
R_{SD}	Reflectance of the Secchi disk	Dimensionless
R_∞	Reflectance of the environment around the Secchi disk	Dimensionless
W	Wind speed	$m.s^{-1}$
Z_{SD}	Secchi disk depth	m
$\alpha_{490-560}$	Proportionality factor between the residual absorption at 490 and 560 nm	Dimensionless
γ	Coupling constant	Dimensionless
ρ_w	Irradiance reflectance	Dimensionless
$\bar{\rho}$	The (air–water) Fresnel reflectance at the interface that applies to the whole downward irradiance from the sun and the sky	Dimensionless
$\Re_0$		Dimensionless
$\rho(\theta',\theta)$	Fresnel reflectance for the associated directions θ and θ′	Dimensionless
τ_a	Atmospheric thickness	Dimensionless
θ	Incident direction	
θ'	Refracted direction	
θ_s	Zenith solar angle	
Subscript on IOPs	Signification	
No subscript	Total	
p	Particulate (in the meaning of suspended particulate material)	
w	Water	
^	Estimated variable, e.g. $\hat{K}_d$	

chlorophyll a concentration ([chl *a*], in $mg\,m^{-3}$) and its seasonal evolution (Earth observation era), but also decadal trends in [chl *a*] (Antoine et al., 2005; Martinez et al., 2009).

At present, the algorithms proposed to estimate the ocean transparency from remotely sensed data are empirical. Using ocean color data, Prasad et al.(1998) proposed a relationship between the Secchi depth and the ratio of two water-leaving radiances. This empirical algorithm was calibrated with simultaneous in situ measurements of Secchi depths and water-leaving radiances in the California Current System (CalCOFI database). Kratzer et al.(2003) proposed an empirical relationship with measurements realized in the Baltic Sea to obtain Z_{SD} from the vertical diffuse attenuation coefficient at the wavelength 490 nm ($K_d(490)$ in m^{-1}), which is a standard product for some ocean color sensors. In parallel to the ocean color sensors, some imager satellites such as Landsat (suite of satellites launched from 1972 by US agencies), which have a better spatial resolution but a worse radiometric sensitivity than ocean color sensors, have been used to monitor the water clarity in lakes. Kloiber et al.(2002) (and references therein) tested some relationships between the Secchi depth and simultaneous measurement by Landsat sensors. Several combinations of spectral reflectance values and spectral band ratios were tested and a sensitivity analysis provided an optimal form for all images. However, Kloiber et al.(2002) could not obtain a standard relationship with coefficients valid for all images, which shows the limits of empirical algorithms, in the case of visible imagery.

Table 2
Summary of the in situ Secchi disk depths data obtained for various locations, with the minimum depth, the maximum depth and the number of measurements.

Geographical zone	Data provider	Date	Min–max (number)
NW Mediterranean Sea (Elbe)	EPSHOM	29/05/03–17/06/03	18–21(6)
NW Mediterranean Sea	Dyfamed	20/01/02–17/10/06	7–29 (37)
NW Mediterranean Sea	Boussole	25/03/05–07/09/06	7–25 (21)
Bay of Biscay	EPSHOM	07/10/02–19/10/02	3–16 (45)
		27/03/03–10/04/03	1.3–16.5 (75)
		13/10/04–24/10/04	1–19 (55)
Skagerrak and Kattegat	IMR	14/04/04–29/04/04	2–15 (82)
North Sea	BSH	28/07/03-12/08/03	2.3-18(52)
North Sea	BSH	05/08/04-18/08/04	2-15(46)
English Channel	EPSHOM	01/09/04	0.05–5.5 (15)
South Pacific	Biosope	21/10/04–09/12/04	10.5–70 (20)
Off California	CALCOFI	02/07/02–26/01/08	1–41 (634)

Comparatively to empirical algorithms, the semi-analytical algorithms use approximations of the radiative transfer that relate inherent optical properties (IOPs), and apparent optical properties (AOPs) or radiometric quantities, in addition to empirical relationships. They tend to catch part of the physics underlying variations in ocean color (IOCCG, 2006). The advantage of using semi-analytical algorithms is that most parameters of the algorithms can be measured or calculated, and are documented in the literature. Many of the semi-analytical algorithms proposed during the last decade are described and tested in IOCCG(2006). More recently, Doron et al.(2007) proposed a semi-analytical algorithm for the estimation of the vertical diffuse attenuation coefficient K_d and the beam attenuation coefficient c (m^{-1}) for both oceanic and turbid waters. Its validation was conducted with the simultaneous measurements at sea of IOPs and AOPs, c, K_d, and the irradiance reflectances R (dimensionless) for various waters, including estuarine, coastal and oceanic ones. Since a tight relationship exists between Z_{SD} and $K_d + c$, it is possible to adapt this semi-analytical algorithm to estimate the ocean transparency from ocean color satelliteborne data.

In the present study, we assess two semi-analytical algorithms: the Quasi-Analytical Algorithm (QAA), developed and published by Lee et al. (2002, 2005a,b) (IOCCG, 2006) and a modified version of the algorithm developed by Doron et al. (2007) to retrieve the Secchi depth from satelliteborne measurements (noted SA). We assess in parallel an empirical algorithm (EMP). The algorithms are comprehensively validated with a large database containing in situ Secchi depth measurements above various water types (coastal and oceanic) and simultaneous satelliteborne data, from the MERIS, MODIS and SeaWiFS sensors. Using ocean color archives, we calculated climatologies of ocean transparency over the North Sea, western Baltic Sea, and Skagerrak and Kattegat straits.

2. Description of the algorithms

In this section, we present the successive steps necessary to convert the spectral radiances measured by the ocean color sensors to the ocean transparency Z_{SD}.

Table 3
Summary of the obtained match-ups (with the SA algorithm) ventilated according to the geographical location. The minimal and maximal in situ values are shown inside the parenthesis.

Geographical zone	Data provider	MERIS	MODIS	SeaWiFS
1—NW Mediterranean Sea (Elbe)	EPSHOM, Dyfamed, Boussole	39 (5.5–40)	56 (5.5–40)	56 (5.5–40)
2—Bay of Biscay	EPSHOM	60 (1–19)	92 (1–19)	79 (1–19)
3—Skagerrak and Kattegat	IMR	32 (5–15)	66 (2–15)	59 (2–15)
4 North Sea	BSH	51 (2.5–18)	80 (2–18)	82 (2–18)
5 South Pacific	CNRS	7 (21.5–69)	13 (10.5–69)	14 (10.5–46)
6—Off California	CALCOFI	102 (2–37)	126 (2–37)	135 (2–37)
7—English Channel	EPSHOM	15 (0.05–5.5)	13 (1.5–5.5)	13 (0.25–5.5)
total		306	446	438

2.1. Step 1: conversion of remotely sensed radiances to above-water and in-water remote-sensing reflectances and to irradiances reflectances below the surface

A treatment chain for the processing and merging of the ocean color products has been implemented in the framework of the Globcolour project (www.globcolour.info). In this chain, the standard output is the fully-normalized water-leaving radiance $nL_w(0^+, \lambda)$ (in W m^{-2} sr^{-1} nm^{-1}), where nL_w is defined by Mueller and Morel, 2002 as:

$$nL_w\left(0^+,\lambda\right) = L_w\left(0^+,\lambda,\theta,\phi\right)\frac{\overline{F}_0(\lambda)}{E_d(0^+,\lambda)}. \quad (1)$$

In Eq. (1), $L_w(0^+,\lambda,\theta,\phi)$ is the water-leaving radiance above the sea surface (in μW cm^{-2} sr^{-1} nm^{-1}), $\overline{F}_0(\lambda)$ is the extraterrestrial solar spectral irradiance at mean earth-sun distance (in μW cm^{-2} nm^{-1}), and $E_d(0^+,\lambda)$, the downward irradiance can be expressed in the same unity as $\overline{F}_0(\lambda)$ (in μW cm^{-2} nm^{-1}). In Eq. (1), λ (nm) stands for the wavelength dependence and the angles θ and ϕ (in degrees) are the viewing zenith angle and the azimuth angle and stand for the viewing geometry.

By its definition, the above-water remotely-sensed reflectance, $R_{rs}(0^+,\lambda)$ (in sr^{-1}) can thus be easily calculated following Eq. (2).

$$R_{rs}\left(0^+,\lambda\right) = \frac{nL_w(0^+,\lambda)}{\overline{F}_0(\lambda)} \quad (2)$$

And the in-water remotely-sensed reflectance, $r_{rs}(0^-,\lambda)$ (in sr^{-1}) are deduced from $R_{rs}(0^+,\lambda)$ using the equation proposed by Lee et al. (2005a):

$$r_{rs}(0^-,\lambda) = \frac{R_{rs}(0^+,\lambda)}{0.52 + 1.7R_{rs}(0^+,\lambda)} \quad (3)$$

Both $R_{rs}(0^+,\lambda)$ and $r_{rs}(0^-,\lambda)$ are used for the QAA algorithm. Indeed, r_{rs} is calculated at 440, 490, 555 and 670 nm from nL_w and the R_{rs} are calculated as intermediate quantities to estimate $R_{rs}(640)$, which is a necessary for QAA-640 (see Appendix A for details).

The development of the semi-analytical algorithm by (Doron et al., 2007) relied upon the knowledge of the in-water reflectances $R(0^-)$ (dimensionless) derived from the satellite remotely-sensed reflectances ρ_w (in sr^{-1}). By definition, $R(0^-)$ is the ratio of the upwelling irradiance, $E_u(0^-,\lambda)$, to the downwelling irradiance, $E_d(0^-,\lambda)$, right below the sea surface, both expressed in the same units (in μW cm^{-2} nm^{-1} for instance):

$$R(0^-,\lambda) = \frac{E_u(0^-,\lambda)}{E_d(0^-,\lambda)} \quad (4)$$

and ρ_w is defined according to:

$$\rho_w\left(0^+,\lambda,\theta,\phi\right) = \frac{\pi L_w(0^+,\lambda,\theta,\phi)}{E_d(0^+,\lambda)}. \quad (5)$$

Since the relationship between $R(0^-)$ and ρ_w was extensively studied, for instance by Gordon(2005) and Morel and Mueller(2002), we took advantage of the possibility to convert nL_w to ρ_w (Eq. 6) using published results from the literature:

$$\rho_w\left(0^+,\lambda,\theta,\phi\right) = \frac{\pi nL_w(0^+,\lambda)}{\overline{F}_0(\lambda)}. \quad (6)$$

The conversion from R to ρ_w is made following the SeaWiFS protocol document (Morel & Mueller, 2002):

$$\rho_w(\lambda) = \frac{\pi R(0^-,\lambda,\theta_s,IOPs)}{Q(0^-,\lambda,\theta',\phi,\theta_s,\tau_a,W,IOPs)}\left[\frac{1-\overline{\rho}(\theta_s)}{1-\overline{r}R(0^-,\lambda,\theta_s,IOPs)}\frac{1-\rho(\theta',\theta)}{n^2}\right] \quad (7)$$

where θ and θ' are the incident and refracted viewing angles (in °), Q (dimensionless) is the bidirectional factor, θ_s is the solar zenith angle (°), τ_a stands for the atmospheric optical thickness (dimensionless), W for the wind speed (m s^{-1}), IOPs for the inherent optical properties, which here are mainly the absorption coefficient and the backscattering coefficient, $\rho(\theta',\theta)$ is the Fresnel reflection for the collimated beams at the associated directions θ and θ', n is the refractive index of seawater, $\overline{r}$ is the mean (water–air) Fresnel reflectance for the whole diffuse upward flux, and $\overline{\rho}$ stands for the (air–water) Fresnel reflection at the interface that applies to the whole downward irradiance from the sun and the sky. The value of $\overline{r}$ is about 0.48 (Morel & Mueller, 2002).

Gordon(2005) studied extensively the variations of the term $\frac{(1-\overline{\rho}(\theta_s))(1-\rho(\theta',\theta))}{n^2}$ and found its value to be very close to 0.529 for very large variations in wind conditions and solar angles. This value is hereafter noted $\Re_0$ and Eq. (7) simplifies to Eq. (8).

$$\rho_w(\lambda) = \frac{\pi R(0^-,\lambda,\theta_s,IOPs)}{Q(0^-,\lambda,\theta',\phi,\theta_s,\tau_a,W,IOPs)}\left[\frac{\Re_0}{1-\overline{r}R(0^-,\lambda,\theta_s,IOPs)}\right] \quad (8)$$

Table 4
Main statistical quantities for the different sensors (MERIS, MODIS and SeaWiFS) and the QAA, SA and empirical algorithms (based on match-ups for all regions).

	R^2	RMS	Bias	Mean ratio	Mean percent diff	Median percent diff	Min in situ	Max in situ	Min sat	Max sat
MERIS QAA	0.63	14.58	11.77	2.39	140.59	1100.93	0.05	69.00	1.77	68.28
MERIS SA	0.54	8.05	4.44	1.79	87.23	522.55	0.05	69.00	1.57	43.81
MERIS EMP	0.68	5.54	0.97	1.42	60.07	314.81	0.05	69.00	1.34	38.69
MODIS QAA	0.52	15.17	12.06	2.23	126.09	1093.30	1.00	69.00	1.39	80.77
MODIS SA	0.57	8.90	6.29	1.74	78.83	645.29	1.00	69.00	1.65	55.80
MODIS EMP	0.72	5.04	0.89	1.15	33.05	244.45	1.00	69.00	1.26	41.88
SeaWIFS QAA	0.50	15.93	12.64	2.25	128.04	1109.21	0.25	70.00	0.19	79.67
SeaWIFS SA	0.60	9.25	6.86	1.74	78.16	639.25	0.25	46.00	1.65	55.51
SeaWIFS EMP	0.73	5.10	1.44	1.16	33.43	251.10	0.25	46.00	1.22	42.46

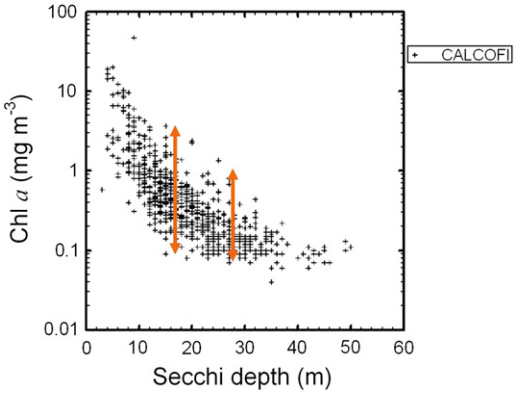

Fig. 1. Scatterplot of Z_{SD} versus [chl *a*], for in situ measurements captured during the Calcofi campaigns.

Using Eq. (8), one can easily calculate R from ρ_w, provided the knowledge of the variations of Q, relatively to the illumination condition, the IOPs and so on. Loisel and Morel, 2001 studied the variations of Q for two very different types of Case 2 waters (optically complex waters, Morel & Prieur, 1977), one sediment-dominated and the other yellow-substance-dominated, and (Park & Ruddick, 2005) proposed to model the value of Q, using numerous radiative transfer simulations. In the present study, the value of 4 for Q has been adopted, because the algorithm was found to be poorly sensitive to the value of Q. Finally, we use Eq. (9) to retrieve R from ρ_w, and Eq. (10) to retrieve R from nL_w.

$$R = \frac{Q\rho_w}{\pi\Re_0 + Q\bar{r}\rho_w} \tag{9}$$

$$R = \frac{QL_{wn}}{\Re_0\bar{F}_0 + Q\bar{r}L_{wn}} \tag{10}$$

The reflectances $R(0^-)$ are used as inputs for both the semi-analytical algorithm presented below and the empirical algorithm also proposed in the present study.

2.2. Step 2: estimation of a(490) and b_b(490) from the spectral $R_{rs}(0^+, \lambda)$ with the QAA method

A first possibility to calculate the absorption coefficient $a(490)$ and the backscattering coefficient $b_b(490)$, both in m^{-1}, from the spectral $R_{rs}(0^+, \lambda)$ is to use the QAA algorithm developed by Lee and co-workers. Since this algorithm has been implemented in slightly different versions in different papers, the equations we used here are gathered in the Appendix A. The input data for this algorithm are the ocean reflectances at four wavelengths: 440, 490, 555 and 670 nm. There may be slight variations in the nominal center of the wavebands due to the technical specifications of each of the satellite sensors.

2.3. Alternative for step 2: use of the adapted semi-analytical algorithm developed by Doron et al.(2007)

A second possibility to calculate $a(490)$ and $b_b(490)$ from two $R(0^-, \lambda)$ is to use the semi-analytical algorithm developed by Doron et al.(2007), noted SA. The inputs of the latter algorithm are the reflectances at two wavebands: one in the visible (490 nm) and the other in the near infrared (709 nm) waveband. The SeaWiFS and MODIS sensors do not perform measurements in the 709 nm waveband and the MERIS sensor data has a low signal-to-noise ratio in the near infrared (NIR) waveband, as viewed during our match-up exercises. This is the reason why, in the present study, we adapted the algorithm of Doron et al.(2007) to use instead two wavelengths λ_1 and λ_2 in the visible (490 and 560 nm). In this adaptation, we use the notation $a_{res}(\lambda)$ to designate the residual absorption coefficient, defined as the total absorption coefficient minus the pure water absorption coefficient: $a_{res}(\lambda) = a(\lambda) - a_w(\lambda)$. We observed in the large database COASTLOOC (described hereafter in the Material and Methods section) that the ratio $a_{res}(490)/a_{res}(560)$ is little variable and we note its value $\alpha_{490-560}$. The other assumption, similar to the one already implemented by Doron et al.(2007) is that the ratio of the backscattering coefficient at the two wavebands 490 and 560 nm is quasi-constant, $B_{490-560} \equiv \frac{b_{bp}(490)}{b_{bp}(560)} = 1.003$.

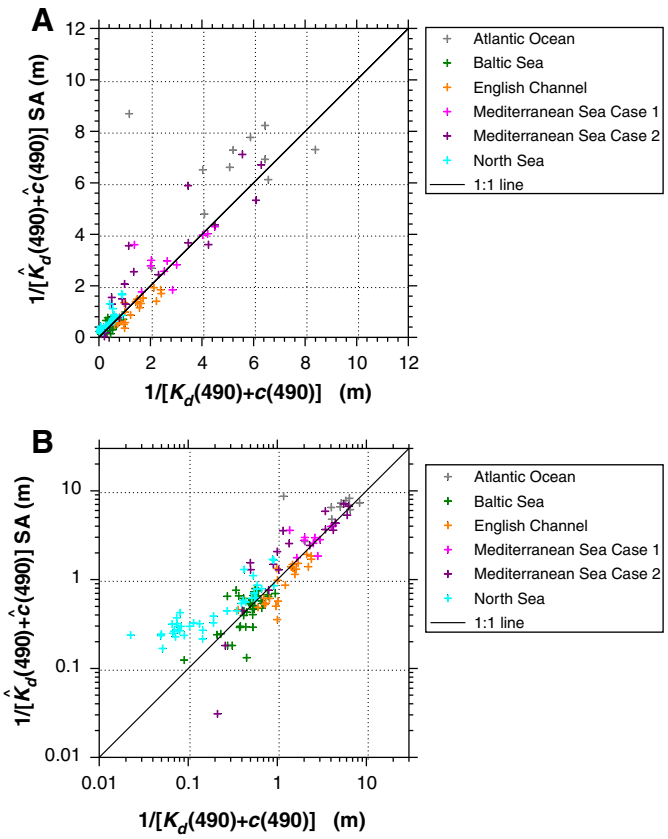

Fig. 2. Relationship between the estimated $\frac{1}{\hat{K}_d(490)+\hat{c}(490)}$ and the measured $\frac{1}{K_d(490)+c(490)}$ for the in situ COASTLOOC dataset. The estimates of $\frac{1}{\hat{K}_d(490)+\hat{c}(490)}$ were obtained with the semi-analytical algorithms using the two wavebands 490 and 560 nm and the determination coefficient R^2 is 0.85. Panel A: in linear scale, Panel B: in logarithmic scale.

The semi-analytical algorithm obtained using this assumption is described with more details in Appendix B, but the final equations are summarized in Eqs. (11) and (12):

$$\begin{cases} b_b(490) = b_{bw}(490) + \dfrac{N}{D} \quad \text{with} \\ N = -B_{490-560}b_{bw}(560) + B_{490-560}\dfrac{a_w(560)}{f(560)}R(560) \\ \qquad + \alpha_{490-560}B_{490-560}\dfrac{f(490)}{f(560)}\dfrac{R(560)}{R(490)}b_{bw}(490) \\ \qquad -\alpha_{490-560}B_{490-560}\dfrac{R(560)}{f(560)}a_w(490) \\ D = 1-\alpha_{490-560}B_{490-560}\dfrac{f(490)}{f(560)}\dfrac{R(560)}{R(490)} \end{cases} \tag{11}$$

$$a(490) = \frac{f(490)\ b_b(490)}{R(490)} \tag{12}$$

In this case, the estimates of $a(490)$ and $b_b(490)$ are obtained using only two irradiance reflectances R (at 490 and 560 nm).

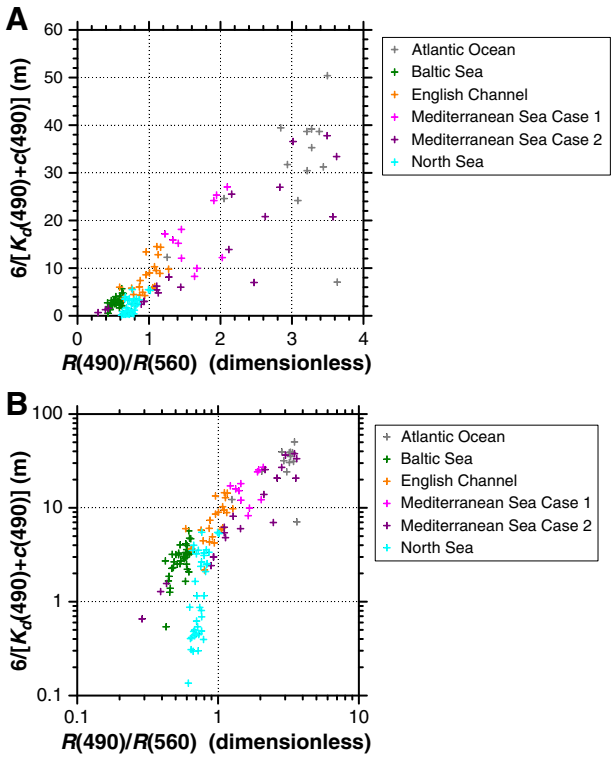

Fig. 3. Scatterplot of the relationship between the ratio of reflectances at 490 and 560 nm and the equivalent of Z_{SD}, here $6/[K_d(490)+c(490)]$, in linear scale (Panel A) and in log scale (panel D).

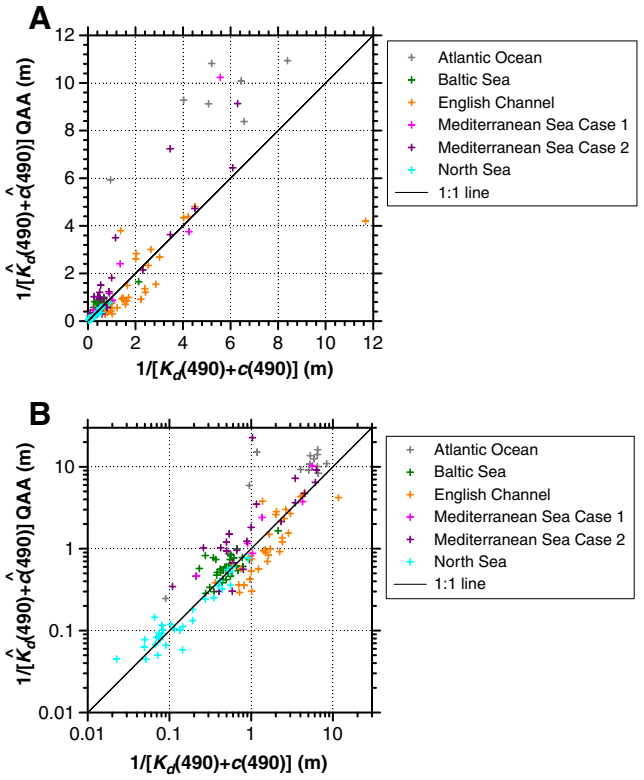

Fig. 4. Relationship between the estimated $\frac{1}{\hat{K}_d(490)+\hat{c}(490)}$ and the measured $\frac{1}{K_d(490)+c(490)}$ for the in situ COASTLOOC dataset, when the estimated values are obtained with the QAA algorithm as explained in the text, in linear scale (Panel A) and log-scale (Panel B).

2.4. Step 3: estimation of $K_d(490)$ and $c(490)$ from $a(490)$ and $b_b(490)$

Once estimates of $a(490)$ and $b_b(490)$ (either with the QAA or the SA) are obtained, Eq. (11) from Lee et al.(2005a) was used to estimate $K_d(490)$ from $a(490)$, $b_b(490)$ and the solar zenith angle θ_s above the water (see Eq. 13):

$$\hat{K}_d(490) = (1 + 0.005\,\theta_s)\hat{a}(490) + 4.18\left(1-0.52e^{-10.8\hat{a}(490)}\right)\hat{b}_b(490) \quad (13)$$

Loisel et al.(2007) proposed an empirical relationship between the particulate backscattering coefficient b_{bp} and scattering coefficient b_p (in m^{-1}) in coastal areas at the wavelength 650 nm, based on simultaneous in situ measurements, (see Eq. 14).

$$b_{bp}(650) = 0.0137\ b_p(650) + 0.00045 \quad (14)$$

Using data from the in situ bio-optical database COASTLOOC, and considering the measured scattering coefficient $b_p(490)$ versus the estimates of $b_{bp}(490)$, obtained with our semi-analytical algorithm, shows that their fit agrees well over the range of values covered by their dataset ($b_p(650)$ between 0.2 and 4 m^{-1}).

2.5. Step 4: the Secchi depth equation

According to Tyler(1968) and Preisendorfer(1986), the Secchi depth Z_{SD} can be expressed by an equation that describes the photopic contrast reduction for a vertical path of sight in a homogeneous medium (Eq. 15):

$$Z_{SD} = \frac{ln\left(\frac{C_0}{C_{min}}\right)}{K_d(v) + c(v)} = \frac{\gamma_0}{K_d(v) + c(v)} \quad (15)$$

where $c(v)$ is the visual photopic beam attenuation coefficient (in m^{-1}), $K_d(v)$ is the visual photopic vertical diffuse attenuation coefficient of the medium (in m^{-1}), (here v stands for visual), C_0 is the inherent contrast between the disk and background water, C_{min} is the minimum apparent contrast perceivable by the human eye under daylight (both contrasts are dimensionless), and γ_0 is the coupling constant (dimensionless).

Eq. (16) below, obtained by Doron et al.(2007), allows estimating $K_d(v)+c(v)$ from $K_d(490)+c(490)$:

$$P(x) = 0.0989x^2 + 0.8879x - 0.0467 \quad (16)$$

where x stands for $K_d(490)+c(490)$ and $P(x)$ stands for $K_d(v)+c(v)$.

Eq. (15) provides the link between the estimated $[K_d(v)+c(v)]^{-1}$ and the Secchi depth. The contrast can be written as $\gamma_0 = ln\frac{C_0}{C_{min}}$. The inherent contrast, C_0, depends on the optical properties of the disk and of the background water column (Eq. 17), where the R_{SD} is the reflectance of the Secchi disk and R_∞ is the reflectance of the environment:

$$C_0 \equiv \frac{R_{SD} - R_\infty}{R_\infty}. \quad (17)$$

The quantity C_{min} has been measured by Blackwell(1946) and reported by Tyler(1968). Preisendorfer(1986) gives some resulting values of the coupling constant between 5 and 10 for varying conditions. A reasonable value for R_{SD} can be 0.82, since the Secchi disk is painted in white in order to be highly reflective. In this formulation, the calculation of the contrast is not wavelength-specific. Since 490 nm is the wavelength for which the light usually penetrates

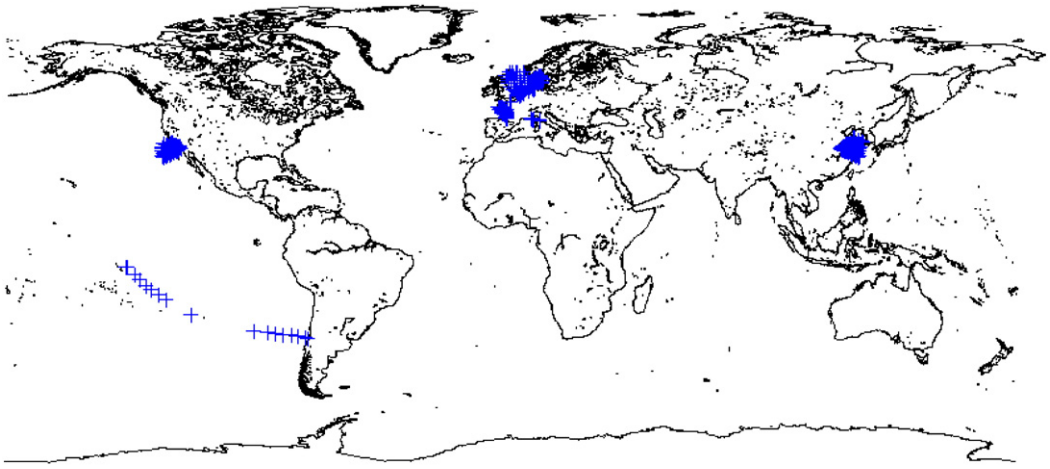

Fig. 5. Map of the spatial distribution of the match-ups.

deeper, we used the reflectance at 490 nm to better reproduce the photopic contrast reduction (Eq. 18).

$$\gamma_0(490) = ln\frac{C_0(490)}{C_{\min}} = ln\frac{\frac{R_{SD}(490)-R_\infty(490)}{R_\infty(490)}}{C_{\min}} \quad (18)$$

2.6. Summary of the different steps of the algorithms

The input quantities are the sun zenith angle θ_s and the nL_w at 440, 490, 555 and 670 nm (QAA) or at 490 and 560 nm (SA) from MERIS, MODIS or SeaWiFS sensors. The reflectances are converted into irradiance reflectances just below surface R or above-water remote-sensing reflectances R_{rs}. The latter quantities are processed to retrieve $a(490)$ and $b_b(490)$ then $K_d(490)$ and $c(490)$. An empirical relationship (second order polynom) is used to estimate $K_d(v)+c(v)$ from $K_d(490)+c(490)$. Z_{SD} is finally obtained by multiplying $\frac{1}{K_d(v)+c(v)}$ by the coupling constant $\gamma_0(490)$, calculated for each station.

2.7. Alternative algorithm: empirical algorithm (EMP)

For practical reasons, an empirical algorithm was developed and it directly links $R(490)$ and $R(560)$ to Z_{SD}. It is based on the observation that, in the in situ dataset, there is a strong relationship between the ratio $R(490)/R(560)$ and $\frac{6}{K_d(490)+c(490)}$, which is a proxy of Z_{SD}. Eq. (19) provides Z_{SD}, from $R(490)$ and $R(560)$, when they are obtained previously from $nL_w(490)$ and $nL_w(560)$.

$$Z_{SD} = 1.888\gamma_0\left(\frac{R(0^-,490)}{R(0^-,560)}-0.52\right) \quad (19)$$

A prior "quality control" is done before applying Eq. (19), which consists in the following criterion: $0.005<R(490)<0.22$, $0.006<R(560)<0.3$ and $0.22<R(560)/R(490)<3.5$. The same criterion is also applied for the SA algorithm. The "quality control" applied to the QAA algorithm is to check the positiveness of the quantities $a(490)$ and $b_b(490)$. The two different sets of quality control for the algorithms may lead to some very small differences in the number of match-ups.

3. Material and methods

To assess the results given by the different algorithms described above, we used different datasets. The first one consists in measurements of bio-optical properties in European coastal waters (COASTLOOC). The second one consists in a large data set of in situ measurements of Secchi disk depths in various places. Simultaneous measurements gathered by the ocean color sensors MERIS, MODIS and SeaWiFS have been considered to obtain a match-up database.

3.1. COASTLOOC dataset

The COASTLOOC dataset has been obtained on more than 400 locations around Europe in coastal and oceanic waters. The measured inherent optical properties (IOPs) have been described by Babin et al.(2003a) for the variations in the absorption coefficient and in Babin et al.(2003b) for the variations in the scattering coefficient. The measurements of the vertical diffuse attenuation coefficient K_d and the irradiance reflectances R have been previously described byDoron et al.(2007). This dataset spans a wide range of natural water conditions: from turbid to clear, and from CDOM-dominated (CDOM stands for colored dissolved organic matter) to NAP-dominated coastal waters (NAP stands for non-algal particles). It is used here to parameterize some of the empirical relationships necessary for the development of the algorithms ($\alpha_{490-560}=a_{\text{res}}(490)/a_{res}(560)$, $B_{490-560}\equiv\frac{b_{bp}(490)}{b_{bp}(560)}$). It also serves to show the validity of the adapted semi-analytical algorithm (using the wavebands 490 and 560 nm).

3.2. In situ measurements

The Secchi disk measurements follow a simple protocol, such as the one described by Preisendorfer(1986). Secchi disk depth measurements were gathered to develop a database of simultaneous in situ and satelliteborne measurements. Historical data cannot be used because

Table 5
Summary of the statistics for the Type II regression between the in situ Z_{SD} and the estimated Z_{SD}. The estimated Z_{SD} can be calculated with three different sensors and with different algorithms (QAA, SA and empirical).

	A = Type II intercept	SD(A)	B = Type II slope	SD(B)
MERIS QAA	5.79	1.09	1.45	0.10
MERIS SA	5.09	0.69	0.96	0.07
MERIS EMP	1.80	0.61	0.95	0.06
MODIS QAA	6.34	1.04	1.43	0.10
MODIS SA	5.48	0.70	1.06	0.06
MODIS EMP	0.17	0.56	1.05	0.05
SeaWIFS QAA	6.24	1.08	1.46	0.10
SeaWIFS SA	3.95	0.56	1.22	0.05
SeaWiFS EMP	−0.84	0.40	1.17	0.04

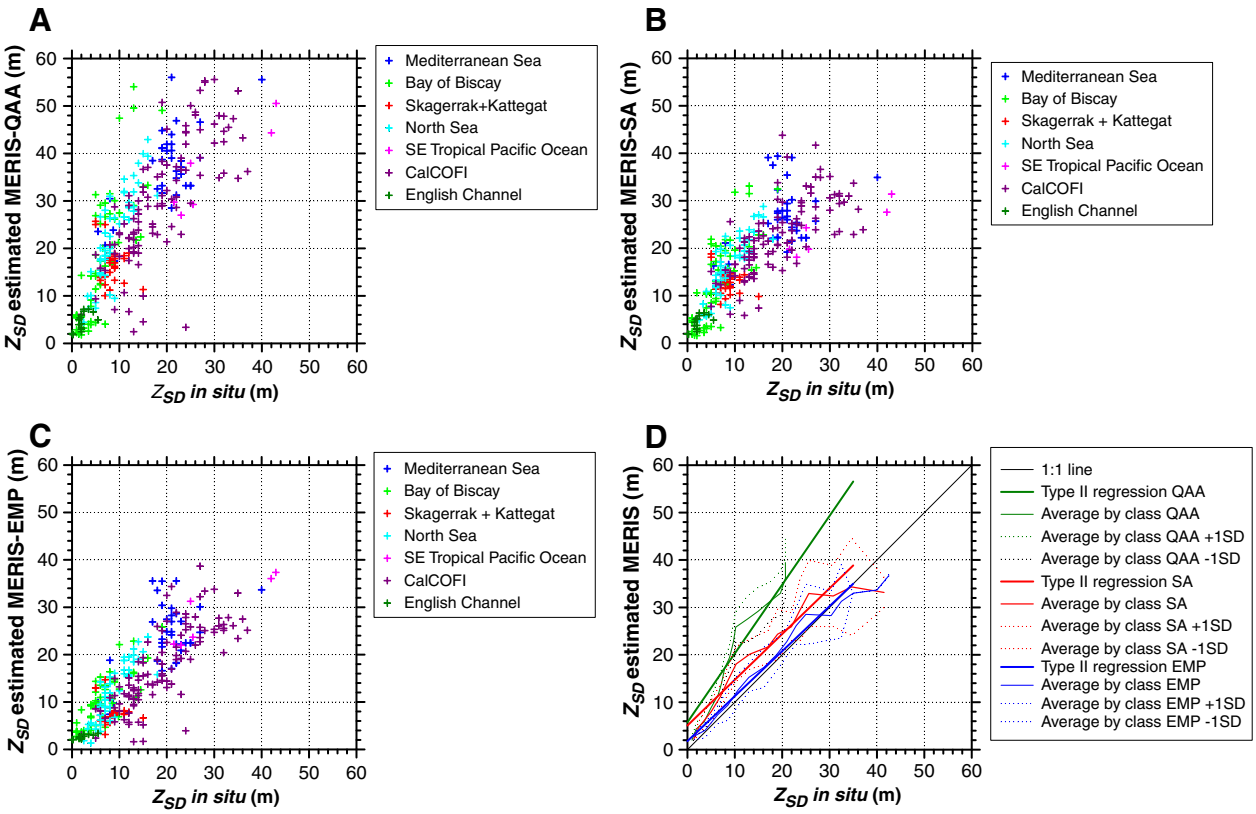

Fig. 6. Scatterplots of the estimated $\hat{Z}_{SD}$ versus in situ Z_{SD}; A) $\hat{Z}_{SD}$ is calculated with the MERIS reflectances and the QAA algorithm; B) $\hat{Z}_{SD}$ is calculated with the MERIS reflectances and the semi-analytical (SA) algorithm; C) $\hat{Z}_{SD}$ is calculated with the MERIS reflectances and the empirical (EMP) algorithm; D) Lineplots of the type II regression for the scatterplot of MERIS –QAA, SA and EMP. The thick lines represent the regression lines, whereas the thin lines represent the average (and +/−SD) by class, with the classes being taken perpendicular to the type II regression line.

of the recent launch of SeaWiFS (1997) and both MERIS and MODIS (during the year 2002). We gathered data from different oceanographic campaigns, to cover various environments such as open and coastal environments, from clear waters to turbid ones. A total of more than 1000 measurements taken after 1st July 2002 are considered over a period of a few years, in the Mediterranean Sea, the Bay of Biscay, the English Channel, the North Sea, the Skagerrak and Kattegat straits, the Californian Current System, and the tropical South East Pacific Ocean. Table 2 provides a summary of in situ measurements by name of the campaigns, and the number of measurements, the minima and maxima in measured values, and the date of measurements.

3.3. Match-ups with remotely sensed ocean color data: MERIS, MODIS and SeaWiFS

For the present study, the nL_w from the Globcolour project were used for the three sensors. The initial data were provided by the European Space Agency (ESA) for the MERIS sensor and by the NASA for the MODIS and SeaWiFS data. All data were then processed by the company ACRI-ST (Sophia Antipolis, France).

A match-up is here defined as an in situ measurement made simultaneously with a remote sensing one. To get a substantial number of match-ups, we considered that the temporal simultaneity was achieved as long as the delay between the in situ measurement and satellite overpass was less than two days. To reduce the pixel-to-pixel natural variability, we considered not only the closest pixel, but also any pixel within a distance of 9 km. A given ensemble of pixels (i.e. the valid pixels within a distance of 9 km from the in situ measurement) is called here a macro-pixel. Our definition of a match-up may seem loose, but with this approach, we obtained finally only 306 match-ups with MERIS images and the SA algorithm. There are respectively 446 and 438 match-ups with MODIS and SeaWiFS images for a total of more than 1000 in situ measurements. We know we add some scatter to the data due to these spatial and temporal ranges, but in the same time for waters with reasonable spatial and temporal variability, it allows to gather more data and have some statistics. In the future, it will be possible, as more and more match-ups will be gathered to refine the time lag between the measurements at sea and the satellite measurements and possibly to quantify the scatter of the retrieval due to the spatio-temporal mismatch. We note that there are systematically more match-ups with the MODIS and SeaWiFS sensors than with the MERIS sensor because they have a larger swath than the MERIS sensor and have a different quality control, probably less restrictive. In addition, MERIS is often affected by sunglint.

4. Results and discussion

In this section, we assess the performance of three algorithms (QAA, SA and EMP) with the three different sensors. First, we use the in situ COASTLOOC data set to assess the ability of the SA described in the Appendix B, to retrieve $[K_d(490)+c(490)]^{-1}$ with the reflectances at 490 and 560 nm instead of 490 and 709 nm as originally published by Doron et al.(2007). Second, we present the results from match-up comparisons between Secchi depths estimated using the three algorithms from remote sensing data, and measured in situ. The algorithms are tested for MERIS, MODIS and SeaWiFs data. For each comparison, we provide a number of statistics to allow a comprehensive comparison between algorithms: determination coefficient R^2, RMS, bias, mean ratio, mean percent difference, median percent difference, and minimum and maximum values for estimates and in situ data (see Table 3). We also provide the Type II regression intercept and slope with their associated error bars, following Isobe et al.(1990)

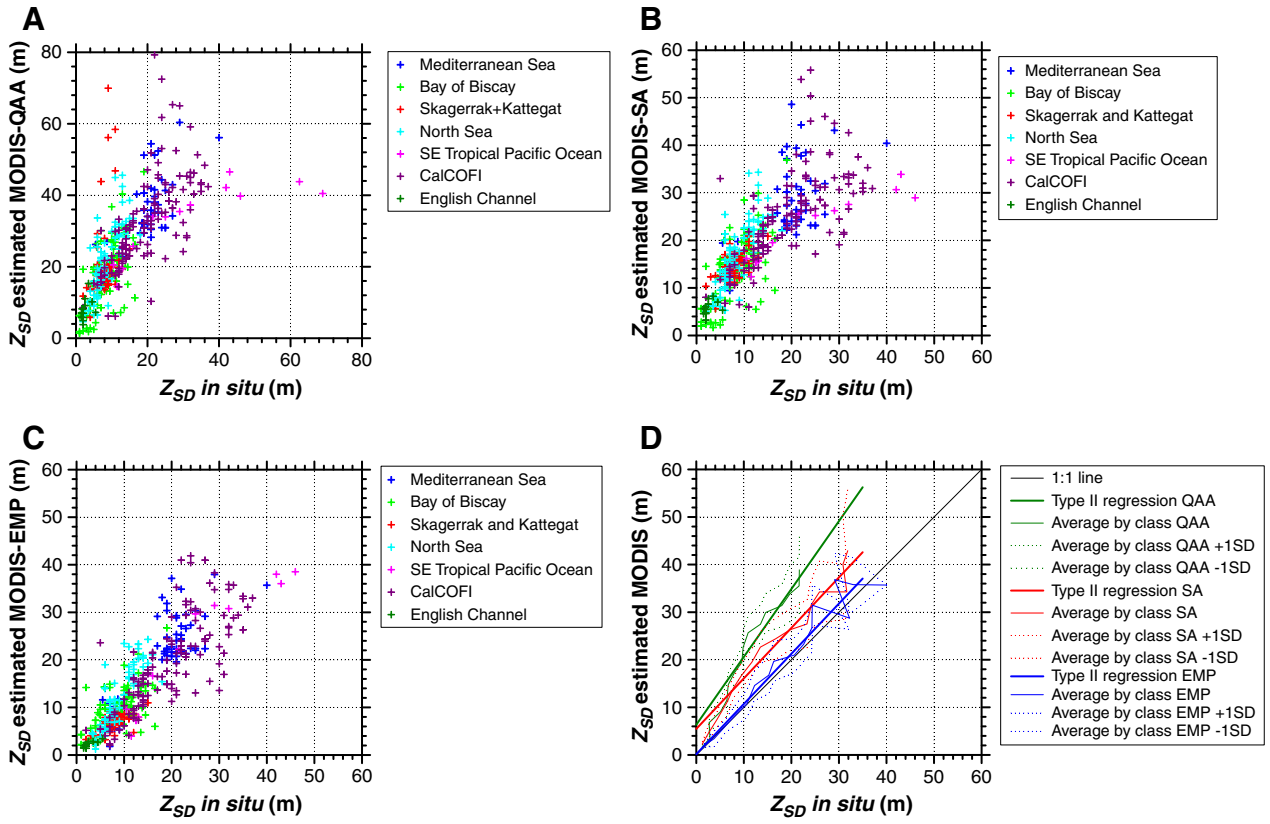

Fig. 7. Scatterplots of the estimated $\hat{Z}_{SD}$ versus in situ Z_{SD}; A) $\hat{Z}_{SD}$ is calculated with the MODIS reflectances and the QAA algorithm (note that for this scatterplot, the scale is different from the other plots scale and ranges from 0 to 80 m); B) $\hat{Z}_{SD}$ is calculated with the MODIS reflectances and the semi-analytical (SA) algorithm C) $\hat{Z}_{SD}$ is calculated with the MODIS reflectances and the empirical (EMP) algorithm; D) Lineplots of the type II regression for the scatterplot of MODIS –QAA, SA and EMP. The thick lines represent the regression lines, whereas the thin lines represent the average (and +/−SD) by class, with the classes being taken perpendicular to the type II regression line.

(see Table 4). This aims to precisely quantifying the performances of the algorithms. All the equations used to calculate these statistical quantities are detailed in Appendix C.

4.1. Why trying to go directly from ocean color reflectances to Secchi depth?

Several previous studies took advantage of the strong relationship between the chlorophyll *a* concentration ([chl *a*]) and the Secchi depth generally observed in oceanic waters, to address biogeochemistry problems. For instance, Simonot and Le Treut(1986) used an empirical approach to convert the historical Secchi depth into [chl *a*] to investigate the potential variations in the phytoplanktonic content at decadal timescales. Such an empirical relationship was also used by Lewis et al.(1988) to investigate the variations in the primary productivity. In the way around, Morel et al.(2007) proposed an empirical algorithm to derive the Secchi depth from ocean color in Case 1 waters, which uses a [chl *a*]-based empirical parameterization. None of those approaches are valid for coastal (so-called Case 2) waters, because the Secchi depth in such waters is strongly affected by resuspended particles, and by the dissolved and particulate material brought by rivers, in addition to phytoplankton and covarying optically significant material. Fig. 1 illustrates this assertion. It shows a scatterplot of Z_{SD} versus [chl *a*] for a large and consistent dataset collected over many years in the frame of the Calcofi program (www.calcofi.org). Measurements from the Calcofi program can be considered as being both from Case 1 (oceanic) and Case 2 (coastal) waters, where Case 1 and Case 2 waters have been defined by Morel and Prieur(1977). Large variations in Z_{SD} are found for a given [chl *a*] and reciprocally in [chl *a*] for a given Z_{SD}, although all measurements are coincident and performed simultaneously at sea, which avoids a number of sources of error (e.g. spatial and temporal mismatch, atmospheric corrections).

4.2. Validation of the algorithms on the COASTLOOC dataset

The advantage of the COASTLOOC dataset is that it includes simultaneous measurements of IOPs (such as *c*) and AOPs (K_d and *R*), but unfortunately, and due to the protocol used (most measurements carried out from an helicopter platform), it contains no Secchi depth measurements. This prevents us from testing directly the algorithms examined here with simultaneous Secchi depth measurements. With this dataset, we assess the quality of the retrieval of the optical quantity $[K_d(490)+c(490)]^{-1}$ with the QAA (see Appendix A), the semi-analytical algorithm modified from Doron et al.(2007) (SA algorithm, see Appendix B) and the empirical algorithm (EMP).

Fig. 2 shows the scatterplot of estimated versus measured $[K_d(490)+c(490)]^{-1}$. A very good agreement is found with a determination coefficient R^2 of 0.85, and no regional bias except for the North Sea at very low Secchi depth values. Because all variables (*R*, K_d anc *c*) are subject to measurement errors, we consider the statistical results from Type II linear regresssions. The slope and intercept are respectively 1.04 and 0.053. Fig. 3 shows the scatterplot of $6/[K_d(490)+c(490)]$, which is a good approximate of Z_{SD}, versus the ratio of the reflectances at 490 and 560 nm, which forms the basis of the EMP algorithm. One can see in Fig. 3A, in linear scale a good correspondence between the two quantities, whereas it is less satisfactory, when observed in log-scale, for instance with ratios with value lower than 1. Fig. 4 shows the scatterplot obtained when considering the QAA results on the COASTLOOC dataset. The results of QAA are equivalent of the SA algorithm, as was already noticed by Doron et al.(2007). The comparison between the three algorithms on the in situ dataset is complementary from the comparisons of their results for the

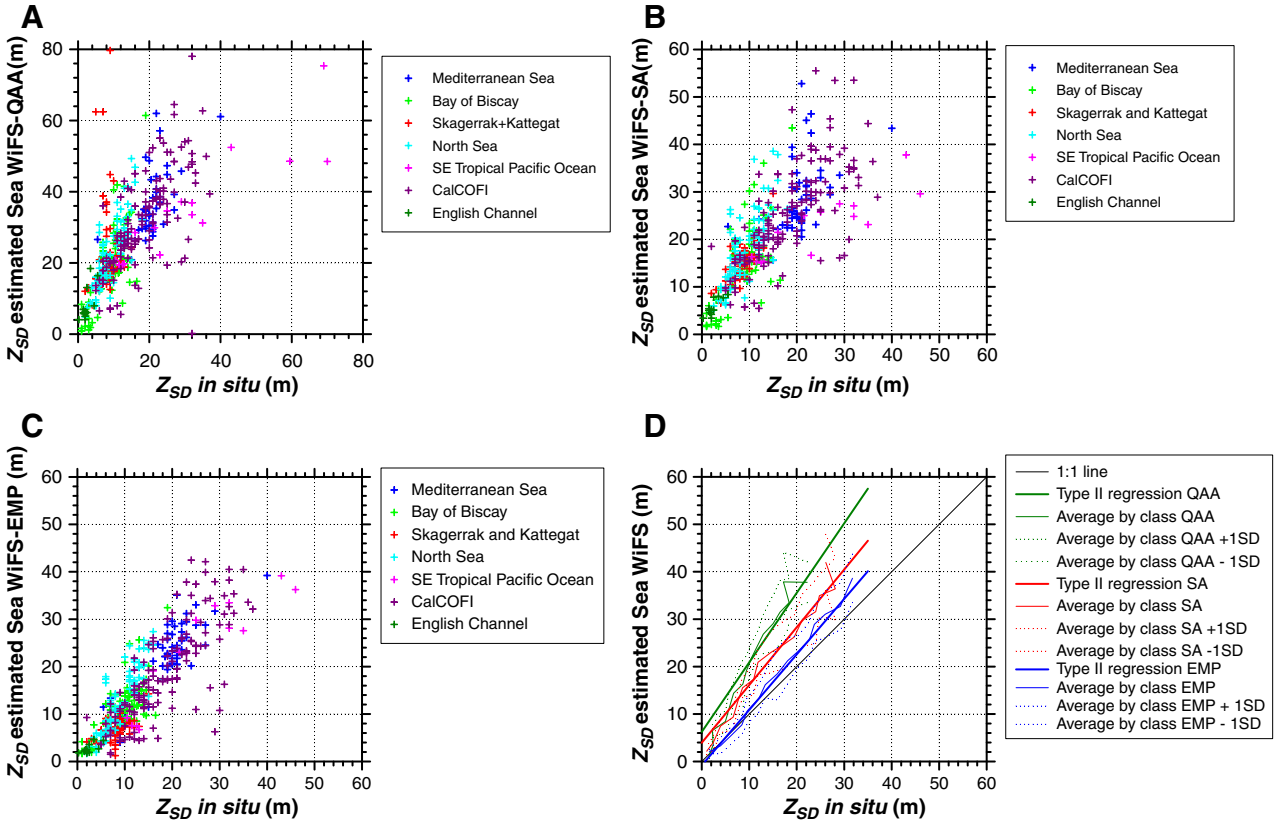

Fig. 8. Scatterplots of the estimated $\hat{Z}_{SD}$ versus in situ Z_{SD}. A) $\hat{Z}_{SD}$ is calculated with the SeaWiFS reflectances and the QAA algorithm (note that for this scatterplot, the scale is different from the other plots scale and ranges from 0 to 80 m); B) $\hat{Z}_{SD}$ is calculated with the SeaWiFS reflectances and the semi-analytical (SA) algorithm C) $\hat{Z}_{SD}$ is calculated with the SeaWiFS reflectances and the empirical (EMP) algorithm; D) Lineplots of the type II regression for the scatterplot of SeaWiFS –QAA, SA and EMP. The thick lines represent the regression lines, whereas the thin lines represent the average (and +/−SD) by class, with the classes being taken perpendicular to the type II regression line.

satellite dataset. It shows that the three algorithms are efficient in retrieving large values of $[K_d(490)+c(490)]^{-1}$, but they behave differently for low values, for instance in the North Sea (overestimation by SA and underestimation by EMP).

4.3. Validation with in situ Secchi depths measurements

The validity and robustness of an algorithm dedicated to be used at large scale has to be tested under realistic conditions. In our case, the radiance measurements come from satelliteborne ocean color sensors, either MERIS, MODIS or SeaWiFS. To assess the quality of the estimation of ocean transparency, it was necessary to compare Z_{SD} estimated from the satellite data and the simultaneous in situ measurement. This approach with match-ups allows a full validation of the transparency algorithms (including our estimation of the contrast), which was not possible with the COASTLOOC dataset. However, it does imply additional sources of error. First, when using remotely sensed data, one has to rely upon the quality of the atmospheric corrections. The signal from the ocean produces around 10% of the signal measured at the top of the atmosphere for clear waters (Morel, 1980), and the atmospheric corrections are a non-negligible source of error in the retrieval of the water-leaving radiances. There is currently no consensus on how to perform accurate atmospheric corrections over turbid waters (Lavender et al., 2005; Moore et al., 1999; Ruddick et al., 2000; Stumpf et al., 2003). Second, there is some spatial and temporal mismatch between in situ and satellite measurements, amplified in coastal waters because of the high spatial patchiness combined with the often-intense dynamics. Third, the size of one pixel seen from space is around 1 km^2 large and one in situ measurement might not be representative of the entire pixel or macro-pixel. Fourth, Secchi measurements, although easy to perform, are subject to measurement errors and uncertainties. Compared with the use of only in situ optical data, the combined use of ocean color satellite data and in situ data for validation purpose thus involves additional sources of error. Therefore, algorithm validation presented here is the most conservative.

Table 3 provides the number of match-ups used for the validation according to their geographical area. We narrowed down our data set to $N_1 = 306$ match-ups for MERIS, $N_2 = 446$ match-ups for MODIS and $N_3 = 438$ match-ups for SeaWiFS, while starting from more than 1000 Secchi depth measurements. A few outliers were discarded based on the observation of corresponding images (true color compositions), which showed areas largely covered with clouds with small openings, which is a probable reason for the bad quality of the input data. Fig. 5 shows the location of the match-ups on a global map.

For each couple {sensor, algorithm}, we show how estimated and measured Secchi depth compare with a scatterplot, and we provide related statistics as described above and in Appendix C. Results are given in Table 4. In addition, to compare graphically the performance of the three different algorithms, we draw on a single plot the regression lines for the QAA, SA and EMP algorithms. We also show the average match per bins of Secchi depths. In the latter case, the matches are taken perpendicular to the regression line as explained in Appendix C. The type II regression coefficients and uncertainties are gathered in Table 5.

Fig. 6 shows the results for the MERIS sensor. The in situ data ranges between 0.05 and 60 m, with only very few points between 40 and 60 m, whereas the satellite data range between 0.4 and 58 for QAA, between 1.2 and 43 for SA and .3 to 38 for EMP. Since there is only one extreme in situ data ($Z_{SD} = 69$ m), the range of the plots often stops at 60 m to focus on the majority of the data. One can see that there is more scatter with the QAA in general and that QAA tends

to overestimate Z_{SD} for large Z_{SD}. The determination coefficients are 0.54 (SA), 0.68 (EMP) and 0.63 (QAA). The QAA tends to overestimate Z_{SD} systematically which drives to a non-negligible intercept of 5.8 m and a large slope of 1.45. The intercept for SA is in the same order of magnitude (5.1 m), but the slope is closer to 1 (0.96). The EMP intercept is lower (1.8 m) and it shows less scatter than both SA and QAA. EMP shows here to be more robust with the satellite data.

Fig. 7 shows similar scatterplots than Fig. 6, but this time, based on the MODIS satellite measurements. With MODIS, the R^2 are respectively 0.57 (SA), 0.52 (QAA) and 0.72 (EMP). Generally, QAA overestimates the large Z_{SD}. The largest scatter of the data is seen with QAA (specially for large Z_{SD}), it reduces for SA and reduces again for EMP. It is as the EMP algorithm was more robust relatively to the uncertainty in the satellite reflectances. With MODIS data, the linear regression line closest to the 1:1 line is obtained with EMP (intercept I = 0.2 m, slope S = 1.05), then with SA (I = 5.5 m, S = 1.06) with the larger deviation experienced by the QAA (I = 6.3 m, S = 1.43).

Fig. 8 shows the results of the estimation of ocean transparency from space with the SeaWiFS data. The results of the three algorithms are consistent with what was previously obtained with the other two sensors, with R^2 of 0.6 (SA), 0.5 (QAA) and 0.73 (EMP). This time, for the three algorithms, the linear regression line slope is significantly

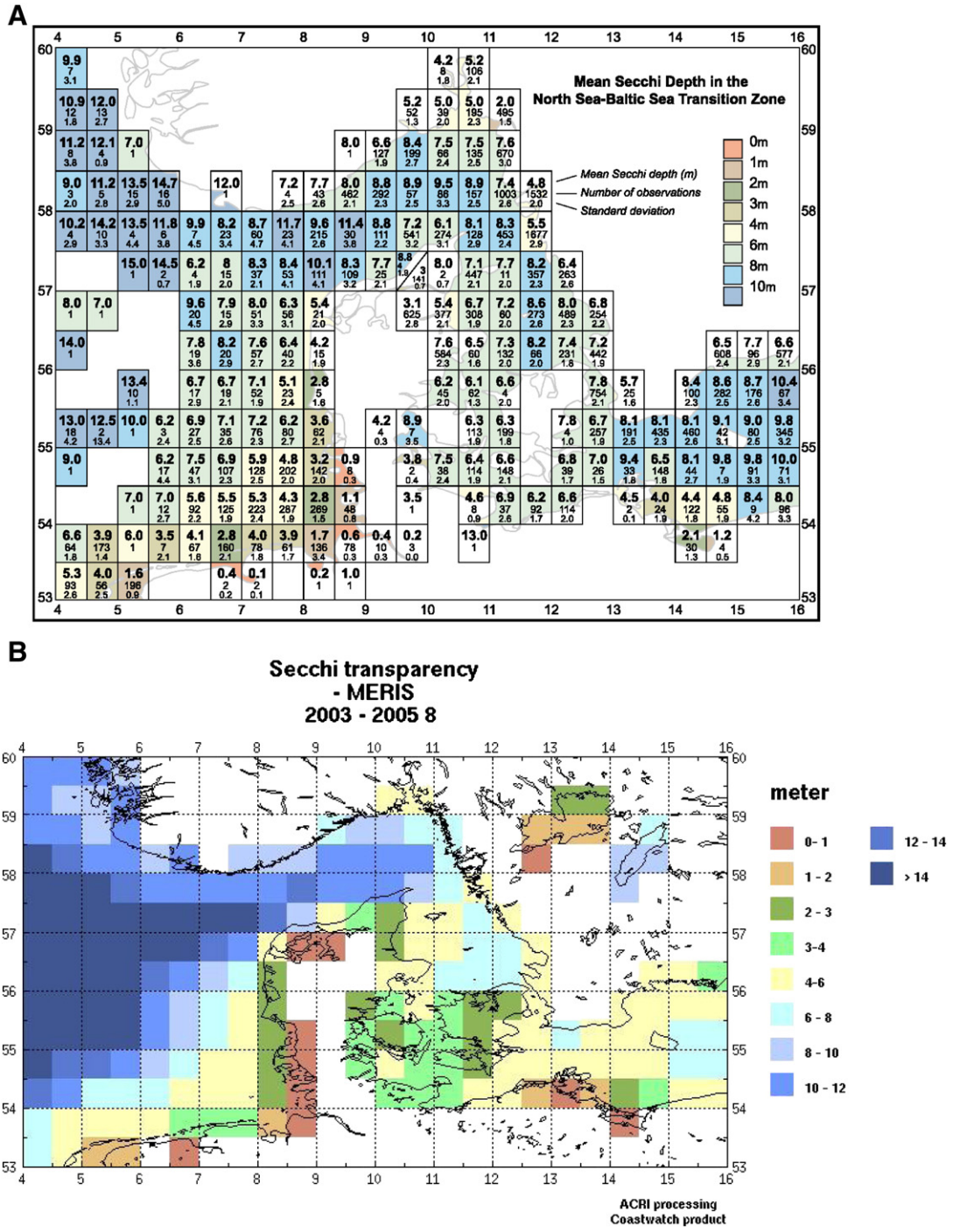

Fig. 9. A Climatology from (Aarup, 2002) obtained with historical Secchi depth in the straits between the North Sea and the Baltic Sea. B. Climatology of the water transparency in the Skagerrak and Kattegat straits over the three years 2003–2005 obtained with the MERIS data and the empirical algorithm. C. Associated standard deviation obtained with the satellite climatology.

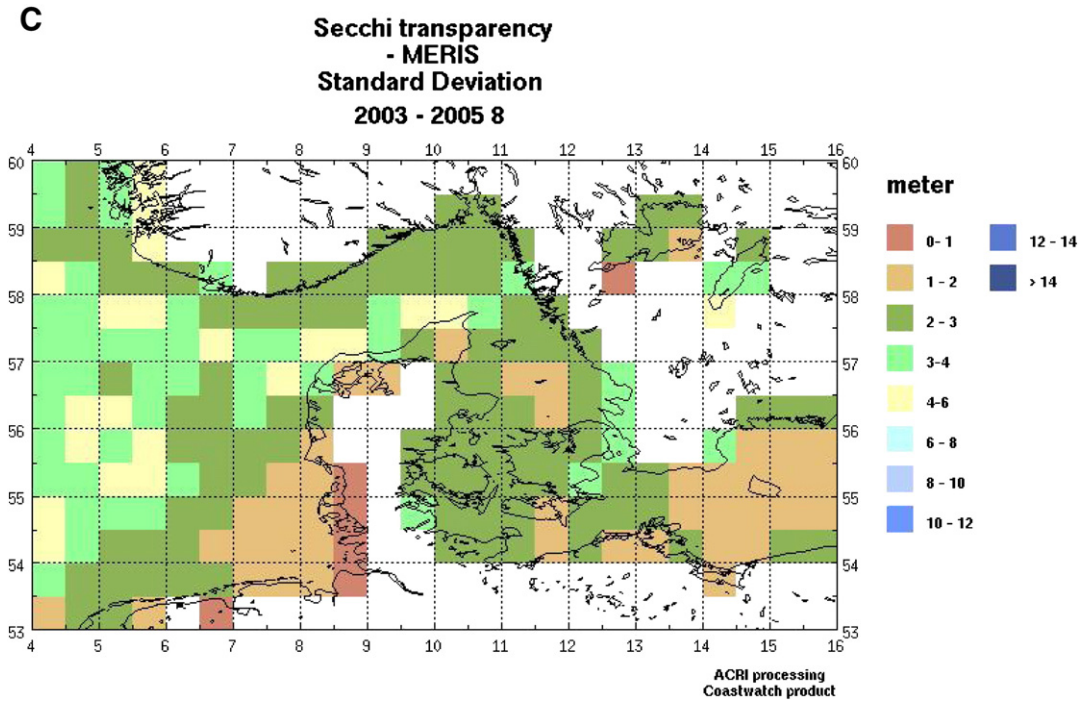

Fig. 9 (*continued*).

larger than 1 and the intercept increases from −0.84 (EMP) to 3.95 (SA) to 6.24 (QAA).

One can note that for ocean transparencies around 10 m in the North Sea and the Bay of Biscay data, there is often a general overestimation for these two regions. It has to be noted that these oceanic regions are well known for their relatively high content in suspended particulate matter (SPM), compared to the open ocean. Failures in atmospheric corrections have been reported by Gohin et al. (2002) in the Bay of Biscay.

Three values of the South Pacific are largely underestimated by the semi-analytical algorithm. The reason might be that, for such very clear waters (more than 40 m of Secchi depth), subtle changes in the properties of the water (beam attenuation and vertical diffuse attenuation coefficient) lead to a large change in the Secchi depth. Our semi-analytical algorithm might not be sensitive enough to grab such changes through the estimation of $K_d(490)$ and $c(490)$ and cannot take into account the vertical variability of these two coefficients. The slight differences between the two sets of quality control for QAA on one hand and SA and EMP on the other hand appear for the clearest stations of the SE Tropical Pacific Ocean. With QAA the clearest in situ stations are 43, 59.5, 69 and 70 m whereas there are only the 43 and 46 m stations with SA and EMP.

In general, the three algorithms perform well in retrieving the ocean transparency from space, though with variations depending on the sensor and the algorithm. The EMP algorithm tends to be rather robust, with larger R^2 and linear regression lines closer to the 1:1 line. The SA algorithm shows more scatter than EMP, has smaller R^2 and linear regression line with non-zero intercepts, although the slope is relatively close to 1. The QAA exhibits systematic overestimation for large Z_{SD}, which in turn impact the regression line.

The development of the SA algorithm has been made with the use of literature data, and in situ bio-optical data (COASTLOOC data set), which means in total independence of the satellite dataset. The comparison of the simultaneous measurements of satellite and in situ ocean transparency directly provides the results described above, without any need to calibrate the data, although there are many sources of uncertainty: radiometric measurements, atmospheric corrections, algorithm sensitivity, in situ measurement errors, spatio-temporal coincidence. The range of validity of the SA algorithm is restricted to the range of the in situ Secchi depth database used for validation purposes, which is between 0.05 m (or more reasonably 1 m) and around 30 m (since only a few measurements were larger than 35 m). Further validation could be completed with an extended dataset including deeper Secchi measurements, but these very transparent waters are less commonly sampled (Megard & Berman, 1989).

Considering the general results given by the three algorithms (QAA, SA and EMP) with the three sensors, as detailed with the statistical quantities, it appears that the EMP algorithm is the least biased. We showed above using the in situ COASTLOOC database that the semi-analytical algorithms (SA and QAA) perform better than the empirical one, especially in being less sensitive to region-to-region differences in the optical behavior. When using satellite data, retrieved water reflectance is affected by error in atmospheric corrections, especially in turbid waters. The semi-analytical algorithms tested here use reflectance ratios and reflectance absolute values. The empirical algorithm tested here only uses a reflectance ratio. The first order error in retrieved reflectance due to bad atmospheric corrections over turbid waters is found in magnitude rather than shape of the reflectance spectrum. This is why the empirical algorithm proves to be more robust when using actual satellite data, and why we use the EMP algorithm in what follows.

4.4. Validation with the climatology over the Skagerrak and Kattegat straits published by Aarup (2002)

Aarup(2002) gathered from local archives past measurements of Secchi depths made in the North Sea and Baltic Sea during the last century and proposed climatologies (annual and seasonal average) of the Skagerrak and Kattegat straits at the resolution of 0.5°. Using the EMP algorithm and all the MERIS data available for the month of August for the years 2003, 2004 and 2005, we calculated the climatology of the ocean transparency over the Skagerrak and Katteg straits, which is the transition zone between the North Sea and the Baltic Sea. Fig. 9A shows the climatology obtained by Aarup(2002) and Fig. 9B shows the average obtained with the EMP algorithm for the three years of data. Both climatologies are represented with the same color code. Fig. 9C displays

the standard deviation obtained over the area with the EMP algorithm. The satellite data show clearly the transition between the coastal areas, surrounding the coast, which have very low ocean transparencies. The orders of magnitude of the data agree well and some seasonal variations can be seen (seasonal climatologies not shown). From the shore to open waters, Z_{SD} increases systematically. It is particularly visible around the shore of Denmark. The North Sea has "clearer" waters of more than 14 m of Z_{SD}, with less variability than coastal waters. The standard deviations are larger in the open ocean than close to the shore. There is a lot more satellite data, even on short time scales, compared to historical data. The historic dataset shows some blank areas with few or no measurements, which occurs rarely with satellite borne sensors. While remote sensing provides much more data than in situ measurements, with larger spatial and temporal variations, the possibility of systematic biases is also increased.

An example of a global map derived from the Globcolour radiance (www.globcolour.info) is shown in Fig. 10 for the month of January 2003. The general features of the ocean are easily recognizable, with the clearer waters in the subtropical gyres for instance. The coastal areas show generally less clear waters, due to the mixture with turbid waters, with resuspension of particulate matters from the bottom or due to large water productivity.

5. Conclusion

In this study, we present a semi-analytical algorithm to estimate the ocean transparency from space with the use of ocean color data. The development of the SA algorithm is totally independent from the satellite dataset on which it is validated. Alternative algorithms: such as the semi-analytical QAA and an empirical (EMP) algorithm are also assessed. The algorithms provide an efficient way of estimating the ocean transparency for three currently flying sensors: MERIS, MODIS and SeaWiFS. This study is one of the very few to actually compare in situ and satellite measurements, including all measurement errors (Melin et al., 2005, 2007; Zibordi et al., 2006).

Among the strengths of the algorithms presented here are the following: two of them are semi-analytical and the recent study by the IOCCG (IOCCG, 2006) proved that the semi-analytical algorithms in general provide better results in the inversion of ocean color signal into biogeochemical quantities for optically complex waters, than empirical algorithms. Additionally, the algorithms proved to be valid over all types of water; and more specifically speaking, there is no sharp boundary between Case 1 and Case 2 waters, which is very convenient for operational purposes. There is also no frontier between geographical regions, except when failures in atmospheric corrections impede the quality of the input data, such as marine radiances. From a practical point of view, the inputs of the algorithms are the normalized water-leaving radiances, which are delivered nearly operationally, for instance in the merging project Globcolour. Hence the algorithms are directly applied on the standard products. The algorithms have proven to be largely validated, since the present satellite validation has been conducted for different water types in various areas around the world and obtained by various investigators. In the present study, one can note that while semi-analytical algorithms provide the most promising results on in situ data, the empirical one proves to be more robust on remote sensing data because it is less sensitive to error due to erroneous atmospheric corrections.

A new climatology of ocean transparency is proposed for the Skagerrak and Kattegat straits. Similarly, new climatologies can be obtained with satelliteborne data to get information about the present state of ocean transparency and to fill the gap between in situ measurements sparsely distributed in time and geographical position. Whenever some historical data are present, the comparison between past and present state could be made, to evaluate any trend in ocean transparency. If available, further assessment of the quality of the algorithm can be done if regional monitoring programs are providing Secchi depth, thus extending the match-up dataset.

Further improvement in the development of the algorithms could take into account the sea roughness through the wind speed (Preisendorfer, 1986) or a better quantification of the bidirectionality factor in the remote sensing data (Park & Ruddick, 2005). As soon as larger datasets will be available, it will also be possible to restrict the time window between measurement time and satellite overpass. This should improve the consistency between measured and estimated Secchi depth, especially in coastal waters for which the timescales are shorter and the patchiness can affect the results. The effect of heterogeneity at the sub-pixel level on the marine reflectance could also help to quantify and understand the error bar on the data.

The present study paves the way to the use of ocean color data operationally for environmental management systems purposes. Ocean transparency, with its proxy Z_{SD}, is mentioned in the European Environmental Agency reports (AEE, 2006), as a quantity used to

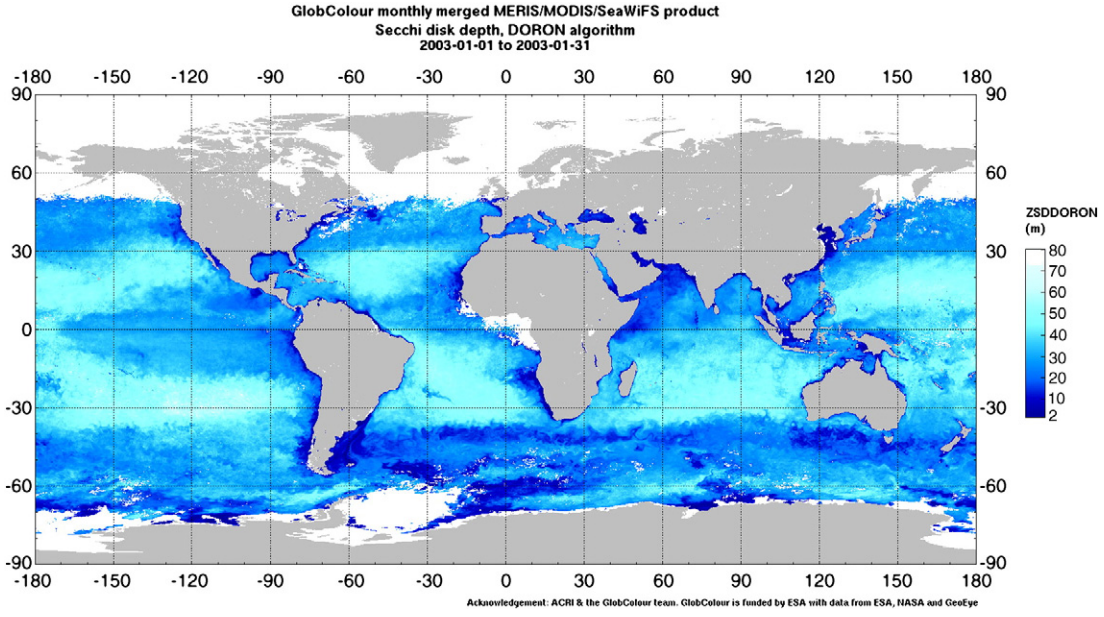

Fig. 10. Average of one month of the Secchi depth at global scale (January 2003), with the Globcolour merged reflectances and the empirical algorithm.

monitor the habitats for instance. It is also a parameter that should be monitored in the European context, with the implementation of the EU Water Framework Directive. Ocean transparency is also used in international programs, such as Helcom, dedicated to the Baltic Sea (see http://www.helcom.fi/environment2/ifs/archive/ifs2007/secchi/en_GB/secchi/).

Acknowledgements

This work has been supported through a PhD fellowship to M. DORON with a CIFRE contract (Association Nationale de la Recherche Technique), and partly funded by the Service Hydrographique et Océanographique de la Marine (SHOM), the ESA GMES Service Element Marcoast and the EU FP7 AQUAMAR (grant agreement 241759).The COASTLOOC project was funded by the 4th Framewok Program of the European Commission. The Secchi disk measurements were provided by California Cooperative Oceanic Fisheries (CalCOFI), Dyfamed (in the framework of the France-JGOFS program), the Bundesamt für Seeschifffahrt und Hydrographie (BSH), the Norvegian Institute of Marine Research (IMR), the EPSHOM. Satellite products were processed and distributed by ACRI-ST GlobColour service, supported by EU FP7 MyOcean & ESA GlobColour Projects, using ESA ENVISAT MERIS data, NASA MODIS and SeaWiFS data.

Appendix A. Details of the implementation of the equations of the QAA (Quasi-Analytical Algorithm), developed by Lee et al. (2002, 2005a,b), IOCCG, (2006)

The QAA has initially been proposed by Lee et al.(2002) and further refined by Lee et al.(2005a), and by Lee et al.(2005b) and also in the IOCCG report on the validation of algorithms developed for optically complex waters (IOCCG, 2006). Since this algorithm has been slightly evolving with time, we recall here all the equations we used in the present paper. The calculations with QAA require that a reference wavelength is chosen. The wavelengths 555 and 640 are recommended by Lee et al.(2002) and to distinguish between calculations made with 555 (640) as the reference wavelength, we will note QAA-555 (respectively 640) and we will also write the reference wavelength as an index in the notation of the physical quantities.

The output of the standard processing scheme, in the Globcolour project, is the fully normalized water-leaving radiance L_{wn} at the wavelengths available for each of the three sensors (MERIS, MODIS and SeaWiFS), as initially introduced by Gordon and Clark (1981). To convert these radiances into above-surface remotely-sensed reflectances R_{rs} (above water), the following equation is used (Morel & Mueller, 2002):

$$R_{rs}(\lambda,\theta_s,\theta_v,\Delta\Phi) = \frac{L_{wn}(\lambda,\theta_s,\theta_v,\Delta\Phi)}{\overline{F}_0(\lambda)}. \quad (A1)$$

In Eq. (A1), L_{wn} (λ, θ_s, θ_v, $\Delta\Phi$) is the normalized water-leaving radiance (in W m^{-2} nm^{-1} sr^{-1}), $\overline{F}_0(\lambda)$is the solar irradiance at the top of the atmosphere at the mean Sun–Earth distance (in W m^{-2} nm^{-1}) and R_{rs} is in sr^{-1}, (defined in Morel & Mueller, 2002). In this equation, λ stands for the wavelength (in nm), θ_s, θ_v, $\Delta\Phi$ are respectively the solar zenith angle, the viewing zenith angle and the azimuth difference between the sun and viewing directions (all three in °).

For MERIS, MODIS and SeaWiFS respectively, the wavelengths and $\overline{F}_0(\lambda)$ used are summarized in Table A1.

The quantities at the heart of the QAA are the in-water remotely-sensed reflectances r_{rs} also in sr^{-1}. The conversion between R_{rs} and r_{rs} is performed following Eq. (A2) (Lee et al., 2002, 2005b) for the four wavelengths 440, 490, 555 and 670.

$$r_{rs}(\lambda) = \frac{R_{rs}(\lambda)}{0.52 + 1.7R_{rs}(\lambda)} \quad (A2)$$

The quantities of interest for us are ultimately $a(490)$ and $b_b(490)$ and a number of intermediate quantities are calculated with Eqs. (A3) to (A9) (summary of equations in Lee et al., 2002 or Lee et al., 2005b). In the following equations, a is the absorption coefficient (in m^{-1}), b_b the backscattering coefficient (in m^{-1}), (with b_{bw} for water and b_{bp} for particles), η is a dimensionless coefficient describing the spectral variations of the particulate backscattering and ν is also a dimensionless coefficient.

$$\nu = ln\left(\frac{r_{rs}(440)}{r_{rs}(555)}\right) \quad (A3)$$

(Lee et al., 2005b)

$$a(440)_i = exp\left(-1.8-1.4\nu + 0.2\nu^2\right) \quad (A4)$$

(Lee et al., 2005b)

$$a(555) = 0.0596 + 0.2\left(a(440)_i - 0.01\right) \quad (A5)$$

(Lee et al., 2005b)

$$u(\lambda) = \frac{-0.0895+\sqrt{0.0895^2 + 4\times 0.1247 r_{rs}(\lambda)}}{2\times 0.1247} \quad (A6)$$

(Lee et al., 2005b)

$$b_{bp}(\lambda) = -b_{bw}(\lambda) + \frac{a(\lambda)u(\lambda)}{1-u(\lambda)} \quad (A7)$$

(Lee et al., 2002)

$$\eta = 2.2\left(1 - 1.2\exp\left(-0.9\frac{r_{rs}(440)}{r_{rs}(555)}\right)\right) \quad (A8)$$

(Lee et al., 2005b)

$$b_b(\lambda) = b_{bw}(\lambda) + b_{bp}(555)\left(\frac{555}{\lambda}\right)^{\eta} \quad (A9)$$

(Lee et al., 2002, 2005b)

First, the application of QAA-555 is done, with 555 nm as the reference wavelength, and allows to estimate $a(555)^{[555]}$, $b_{bp}(555)^{[555]}$, $b_{bp}(490)^{[555]}$, $b_{bp}(440)^{[555]}$, $a(490)^{[555]}$, $a(440)^{[555]}$, using the needed u(λ).

Second, the application of QAA-640 IOCCG, 2006 and Lee et al. (2002) requires the calculation of a (640), according to Eqs. (A10) and (A11).

$$R_{rs}(640) = 0.01R_{rs}(555) + 1.4R_{rs}(670) - 0.0005\frac{R_{rs}(670)}{R_{rs}(490)} \quad (A10)$$

Table A1
Summary of the wavelengths and $\overline{F}_0(\lambda)$ used to calculate R_{rs} from the standard treatment output L_{wn}.

λ	443	490	555	670
$\overline{F}_0(\lambda)$MERIS	187.76098	192.93254	180.04556	153.09105
$\overline{F}_0(\lambda)$MODIS	188.76	194.18	187.00	152.44
$\overline{F}_0(\lambda)$SeaWiFS	188.76	193.38	183.76	151.22

(IOCCG, 2006)

$$a(640) = 0.31 + 0.07\left(\frac{r_{rs}(640)}{r_{rs}(440)}\right)^{1.1} \quad \text{(A11)}$$

(IOCCG, 2006 and Lee et al., 2002)

The knowledge of $a(640)$ allows to calculate $b_{bp}(640)^{[640]}$, $b_{bp}(490)^{[640]}$, and $a(490)^{[640]}$, using the intermediate $u(\lambda)$.

Third, the optimal estimated value for $a(490)$ and $b_b(490)$ is obtained with a linear combination of $a(490)^{[555]}$ and $a(490)^{[640]}$ for $a(490)$ and with a linear combination of $b_{bp}(490)^{[555]}$ and $b_{bp}(490)^{[640]}$ for $b_{bp}(490)$, see Eqs. (A12) and (A13) (IOCCG, 2006).

$$\begin{aligned} a(490) &= a(490)^{[555]} \ \textit{for}\ a(440)^{[555]}<0.3 \\ a(490) &= \left(1-\frac{a(440)^{[555]}-0.3}{0.2}\right)a(490)^{[555]} \\ &\quad +\frac{a(440)^{[555]}-0.3}{0.2}a(490)^{[640]} \textit{for}\ 0.3\le a(440)^{[555]}\le 0.5 \\ a(490) &= a(490)^{[640]} \textit{for}\ a(440)^{[555]} > 0.5 \end{aligned} \quad \text{(A12)}$$

$$\begin{aligned} b_{bp}(490) &= b_{bp}(490)^{[555]} \ \textit{for}\ a(440)^{[555]}<0.3 \\ b_{bp}(490) &= \left(1-\frac{a(440)^{[555]}-0.3}{0.2}\right)b_{bp}(490)^{[555]} \\ &\quad + \frac{a(440)^{[555]}-0.3}{0.2}b_{bp}(490)^{[640]} \textit{for}\ 0.3\le a(440)^{[555]}\le 0.5 \\ b_{bp}(490) &= b_{bp}(490)^{[640]} \textit{for}\ a(440)^{[555]} > 0.5 \end{aligned} \quad \text{(A13)}$$

To conclude this paragraph, it is possible to estimate $a(490)$ and $b_b(490)$ from the value of four remotely sensed reflectances at 440, 490, 555 and 670 nm, with the QAA method. In practical implementations, whenever negative values occurred, whether they were given (radiances) or calculated (intermediate step), the corresponding pixel was discarded.

Appendix B. Adaptation of the (Doron et al., 2007) semi-analytical algorithm using the wavebands 490 and 560 nm

Rationale for using the 560 nm band instead of the 709 nm band

The algorithms to estimate the ocean transparency developed by Doron et al.(2007) require as an input the irradiance reflectances at two wavelengths, 490 and 709 nm. Because the latter wavelength is not available on the MODIS and SeaWiFS sensors and because the MERIS reflectances presented generally a low signal-to-noise ratio at 709 nm (especially in oceanic waters), we considered the possibility of using as an alternative input the reflectance at 560 nm. A critical assumption made by Doron et al.(2007) in the development of their algorithms, was about the dominance of the pure water absorption at 709 nm. This dominance does not hold at 560 nm, but the choice of the 560-nm band is justified by the trough generally observed in the phytoplankton absorption spectrum (for instance, in the absence of some specific pigments, such as the phycoerythrin). The two other optically significant substances, the non-algal particles (NAP) and the colored dissolved organic matter (CDOM) have an absorption spectrum decreasing from the blue to the red wavelengths (Bricaud et al., 1981; Roesler & Perry, 1995). Therefore, the variations of the absorption coefficient at 560 nm of the other substances can be inferred from their absorption coefficient at 490 nm. It allows obtaining a slightly modified version of the semi-analytical algorithms (see below for the equations). Another consideration is the fact that most ocean color sensors measure reflectance at a waveband close to 560 nm.

Despite the relatively small absorption by NAP and CDOM, the assumption of no absorption but the one of pure water does not hold at 560 nm. Residual absorption at 560 nm (i.e. total absorption minus pure water absorption) therefore has to be somehow accounted for in the algorithm of (Doron et al., 2007). The COASTLOOC data set gathers bio-optical data in European coastal waters and oceanic waters (Babin et al., 2003a,b; Doron et al., 2007, see the Material and Methods section for more details). In the COASTLOOC dataset, the residual absorption was calculated as the sum of the absorption of the NAP, the pigments and the CDOM measured with the spectrophotometer (see Babin et al., 2003a). We observed a very tight linear relationship between the residual absorption coefficient at the two wavelengths 490 and 560 nm, which validates the assumption in Eq. (B1). Although the absorption coefficients vary over more than three orders of magnitude, the ratio $a_{res}(560)/a_{res}(490)$ has the average 0.323 with a standard deviation of 0.049 (calculated on 317 values). Thus we can write Eq. (B1)

$$a_{res}(560) = \alpha_{490-560}\,(a_{res}(490)) \quad \text{(B1)}$$

where $\alpha_{490-560}$ is a constant (dimensionless). Given that the backscattering-to-scattering ratio for marine particles, $\tilde{b}_{bp}(\lambda)$, also called the backscattering efficiency, shows very weak spectral variations between 490 and 560 nm (Whitmire et al., 2007), and the spectral variations of the particles observed by Babin et al.(2003b) and Barnard et al.(1998), it is therefore assumed that:

$$B_{490-560} \equiv \frac{b_{bp}(490)}{b_{bp}(560)} = 1.003 \quad \text{(B2)}$$

It was long ago shown that the spectral irradiance reflectance just below the sea surface can be expressed with the following equation (Gordon et al., 1975):

$$R(\lambda) = f(\lambda)\frac{b_{bw}(\lambda) + b_{bp}(\lambda)}{a_w(\lambda) + a_{res}(\lambda)} \quad \text{(B3)}$$

where λ is the wavelength (nm), b_b is the backscattering coefficient (m^{-1}), a is the absorption coefficient (m^{-1}), and the subscripts p, w and a_{res} stand for the particles, water and residual absorption (all elements but the water), respectively (Mobley, 1994).

Using Eq. (B1) to (B3), knowing $R(490)$ and $R(560)$, we have two linear equations and two unknowns ($a_{res}(490)$ and $b_{bp}(490)$), which is a simple system to solve. Finally, it is possible to estimate $\hat{b}_b(490)$ and $\hat{a}(490)$ from $R(490)$ and $R(560)$, assuming $\alpha_{490-560}$, $B_{490-560}$, $f(490)$, $f(560)$ are known (Eqs. (B4) and (B5)). The values of f at both wavelengths are taken equal to 0.335 (average from Loisel & Morel, 2001).

$$\begin{cases} \hat{b}_b(490) = b_{bw}(490) + \dfrac{N}{D} \quad \text{with} \\ N = -B_{490-560}b_{bw}(560) + B_{490-560}\dfrac{a_w(560)}{f(560)}R(560) \\ \qquad + \alpha_{490-560}B_{490-560}\dfrac{f(490)}{f(560)}\dfrac{R(560)}{R(490)}b_{bw}(490) \\ \qquad -\alpha_{490-560}B_{490-560}\dfrac{R(560)}{f(560)}a_w(490) \\ D = 1-\alpha_{490-560}B_{490-560}\dfrac{f(490)}{f(560)}\dfrac{R(560)}{R(490)} \end{cases} \quad \text{(B4)}$$

$$\hat{a}(490) = \frac{f(490)\ \hat{b}_b(490)}{R(490)} \quad \text{(B5)}$$

Appendix C. Equations used to calculate the statistical quantities

To estimate with the higher precision the accuracy of the retrieval of the Secchi depth with each satellite dataset and algorithm, some statistical quantities are systematically calculated for each couple of one algorithm (QAA, SA and EMP) and one dataset (MERIS, MODIS and SeaWiFS). They are gathered in Table 4 and their calculation is detailed hereafter.

$$R^2 = \frac{\left[\sum_{i=1}^{N}(x_i-\overline{x})(y_i-\overline{y})\right]^2}{\sum_{i=1}^{N}(x_i-\overline{x})^2\sum_{i=1}^{N}(y_i-\overline{y})^2} \tag{C1}$$

$$Bias = \frac{1}{N}\sum_{i=1}^{N}(y_i-x_i) \tag{C2}$$

$$RMS = \sqrt{\frac{1}{N}\sum_{i=1}^{N}(y_i-x_i)^2} \tag{C3}$$

$$mean\ ratio = \frac{1}{N}\sum_{i=1}^{N}\frac{y_i}{x_i} \tag{C4}$$

$$mean\ percentage\ difference = \frac{100}{N}\sum_{i=1}^{N}\frac{|y_i-x_i|}{x_i} \tag{C5}$$

$$median\ percentage\ difference = 100 median\ of\left(\frac{|y_i-x_i|}{x_i}\right)_{i=1,N} \tag{C6}$$

In the previous equation, x is the in situ measurement vector and y is the satellite measurement vector (for a given satellite and a given algorithm). In addition, the range of the in situ and satellite measurements are given (minimum and maximum).

An integrated quantity is the equation of the linear regression between the in situ and satellite Secchi depth measurements. Since both quantities are measurements and none is a controlled variable, it is necessary to estimate a type II regression to compare one quantity to the other. A paper by (Isobe et al., 1990) describes comprehensively a few methods to estimate this type II regression and concluded that the OLS (Ordinary Least Square) bisector is the most robust method, when there is uncertainty in both quantities. In addition, this method allows at the same time to have the standard deviation on both the Type II slope and intercept (see Table 5 for the numerical results).

$$y = \mathrm{B}\times + \mathrm{A} \tag{C7}$$

in which B is the slope of the type II regression and A is the intercept of the type II regression.

$$S_{xx} = \sum_{i=1}^{N}(x_i-\overline{x})^2 \tag{C8}$$

$$S_{YY} = \sum_{i=1}^{N}(y_i-\overline{y})^2 \tag{C9}$$

$$S_{XY} = \sum_{i=1}^{N}(x_i-\overline{x})\sum_{i=1}^{N}(y_i-\overline{y}) \tag{C10}$$

$$B(1) = S_{XY}/S_{XX} \tag{C11}$$

$$B(2) = S_{YY}/S_{XY} \tag{C12}$$

$$B(3) = B(1)B(2)-1+\frac{\sqrt{(1+B^2(1))(1+B^2(2))}}{B(1)+B(2)} \tag{C13}$$

$$A(i) = \overline{y}-B(i)\overline{x} \tag{C14}$$

$$GAM(1) = \frac{B(3)}{B(1)+B(2)}\sqrt{(1+B^2(1))(1+B^2(2))} \tag{C15}$$

$$GAM(2) = \frac{B(4)}{\sqrt{(4B^2(1)+(B(1)B(2)-1)^2)}} \tag{C16}$$

$$\hat{x} = x-\overline{x} \tag{C17}$$

$$\hat{y} = y-\overline{y} \tag{C18}$$

$$SUM(1) = \sum_{i=1}^{N}\left(\hat{x}\left(\hat{y}-B(1)\hat{x}\right)\right)^2 \tag{C19}$$

$$SUM(2) = \sum_{i=1}^{N}\left(\hat{y}\left(\hat{y}-B(2)\hat{x}\right)\right)^2 \tag{C20}$$

$$SUM(3) = \sum_{i=1}^{N}\hat{x}\hat{y}\left(\hat{y}-B(1)\hat{x}\right)\left(\hat{y}-B(2)\hat{x}\right) \tag{C21}$$

$$COV = \frac{SUM(3)}{B(1)S_{XX}^2} \tag{C22}$$

$$SIGB(1) = \frac{SUM(1)}{S_{XX}^2} \tag{C23}$$

$$SIGB(2) = \frac{SUM(2)}{S_{XY}^2} \tag{C24}$$

$$SIGB(3) = GAM^2(1)\left(\left(1+B^2(2)\right)^2 SIGB(1) + 2\left(1+B^2(1)\right)\left(1+B^2(2)\right)COV + \left(1+B^2(1)\right)^2 SIGB(2)\right) \tag{C25}$$

$$SIGA(1) = \sum_{i=1}^{N}\left[\left(\hat{y}-B(1)\hat{x}\right)\left(1-\frac{N\overline{x}\hat{x}}{S_{XX}}\right)\right]^2 \tag{C26}$$

$$SIGA(2) = \sum_{i=1}^{N}\left[\left(\hat{y}-B(2)\hat{x}\right)\left(1-\frac{N\overline{x}\hat{y}}{S_{XY}}\right)\right]^2 \tag{C27}$$

$$SIGA(3) = \sum_{i=1}^{N}\left[\left(\hat{x}\left(\hat{y}-B(1)\hat{x}\right)\frac{1+B^2(2)}{S_{XX}} + \hat{y}\left(\hat{y}-B(2)\hat{x}\right)\frac{1+B^2(1)}{S_{XY}}\right)N\overline{x}GAM(1)-\hat{y}+B(3)\hat{x}\right]^2 \tag{C28}$$

The OLS bisector slope and intercept are respectively B(3) and A (3) and they are provided in Table 5. The confidence interval for B is SIGB(3) and the confidence interval for A is SIGA(3).

To better describe the bias par class of values, we calculated the average by class of Secchi depth values (in situ and satellite). Since again, there is uncertainty in both quantities, we use the Type II regression line to define the class. The points are gathered in bins defined perpendicularly to the type II regression line. For each bin, the average of the two quantities (Z_{SD} in situ and satellite) is calculated and both their standard deviation. We then plotted this lineplot on top of the 1:1 line, and the Type II regression line.

References

Aarup, T. (2002). Transparency of the North Sea and Baltic Sea — a Secchi depth data mining study. *Oceanologia*, *44*, 323–337.

AEE (2006), The changing faces of Europe's coastal areas. EEA Report n°6/2006.

Antoine, D., et al. (2005). Bridging ocean color observations of the 1980's and 2000's in search of long-term trends. *Journal of Geophysical Research*, 110 doi:10.1029/2004JC002620.

Babin, M., et al. (2003a). Variations in the light absorption coefficients of phytoplankton, nonalgal particles, and dissolved organic matter in coastal waters around Europe. *Journal of Geophysical Research*, *108*, 3211 doi:10.1029/2001JC000882.

Babin, M., et al. (2003b). Light scattering properties of marine particles in coastal and open ocean waters as related to the particle mass concentration. *Limnology and Oceanography*, *48*, 843–859.

Barnard, A. H., et al. (1998). Global relationships of the inherent optical properties of the oceans. *Journal of Geophysical Research*, *103*, 24955–24968.

Blackwell, H. R. (1946). Contrast threshold of the human eye. *Journal of the Optical Society of America*, *36*, 624–643.

Bricaud, A., et al. (1981). Absorption by dissolved organic matter of the sea (yellow substance) in the UV and visible domains. *Limnology and Oceanography*, *26*, 43–53.

Doron, M., et al. (2007). Estimation of light penetration, and horizontal and vertical visibility in oceanic and coastal waters from surface reflectance. *Journal of Geophysical Research*, *112*, C06003 doi:10.1029/2006JC004007.

Falkowski, P., & Wilson, C. (1992). Phytoplankton productivity in the North Pacific ocean since 1900 and implications for absorption of anthropogenic CO2. *Nature*, *358*, 741–743.

Gohin, F., et al. (2002). A five channel chlorophyll concentration algorithm applied to SeaWiFS data processed by SeaDAS in coastal waters. *International Journal Remote Sensing*, *23*, 1639–1661.

Gordon, H. R. (2005). Normalized water-leaving radiance: revisiting the influence of surface roughness. *Applied Optics*, *44*, 241–248.

Gordon, H. R., & Clark, D. K. (1981). Clear water radiances for atmospheric correction of coastal zone color scanner imagery. *Applied Optics*, *20*, 4175–4180.

Gordon, H. R., et al. (1975). Computed relationships between the Inherent and apparent optical properties of a flat homogenous ocean. *Applied Optics*, *14*, 417–427.

IOCCG ZhongPing Lee (Ed.) (2006), Remote sensing of Inherent Optical Properties: Fundamentals, Tests of algorithms, and Applications, 126 pp., Reports of the International Ocean-Colour Coordinating Group, No. 5, IOCCG, Dartmouth, Canada.

Isobe, T., et al. (1990). Linear regression in astronomy. *The Astrophysical Journal*, *364*, 104–113.

Kloiber, S. M., et al. (2002). A procedure for regional lake water clarity assessment using Landsat multispectral data. *Remote Sensing Of Environment*, *82*, 38–47.

Kratzer, S., et al. (2003). Assessing Secchi and photic zone depth in the Baltic Sea from satellite data. *Ambio*, *32*, 577–585.

Lavender, S. J., et al. (2005). Modification to the atmospheric correction of SeaWiFS Ocean colour images over turbid waters. *Continental Shelf Research*, *25*, 539–555.

Lee, Z. -P., et al. (2002). Deriving inherent optical properties from water color: a multiband quasi-analytical algorithm for optically deep waters. *Applied Optics*, *41*, 5755–5772.

Lee, Z. P., et al. (2005a). A model for the diffuse attenuation coefficient of downwelling irradiance. *Journal of Geophysical Research*, *110*, C02016 doi:10.1029/2004JC002275.

Lee, Z. P., et al. (2005b). Diffuse attenuation coefficient of downwelling irradiance: An evaluation of remote sensing methods. *Journal of Geophysical Research*, 110 doi:10.1029/2004JC002573.

Lewis, M. R., et al. (1988). Global patterns of ocean transparency: Implications for the new production of the open ocean. *Journal of Geophysical Research*, *93*, 6847–6856.

Loisel, H., et al. (2007). Investigation of the optical backscattering to scattering ratio of marine particles in relation to their biogeochemical composition in the eastern English Channel and southern North Sea. *Limnology And Oceanography, Limnology And Oceanography*, *52*, 739–752.

Loisel, H., & Morel, A. (2001). Non-isotropy of the upward radiance field in typical coastal (Case 2) waters. *International Journal Remote sensing*, *22*, 275–295.

Martinez, E., et al. (2009). Climate-driven basin-scale decadal oscillations of oceanic phytoplankton. *Science*, *326*, 1253–1256.

Megard, R. O., & Berman, T. (1989). Effects of algae on the secchi transparency of the Southeastern Mediterranean Sea. *Limnology and Oceanography*, *34*, 1640–1655.

Melin, F., et al. (2005). Assessment of apparent and inherent optical properties derived from SeaWiFS with field data. *Remote Sensing of Environment*, *97*, 540–553.

Melin, F., et al. (2007). Assessment of satellite ocean color products at a coastal site. *Remote Sensing Of Environment*, *110*, 192–215.

Mobley, C. D. (1994). Light and water: Radiative transfer in natural waters. (1st ed.). San Diego, California: Academic Press 592 pp.

Moore, G. F., et al. (1999). The atmospheric correction of water colour and the quantitative retrieval of suspended particulate matter in Case II waters: Application to MERIS. *International Journal Remote Sensing*, *20*, 1713–1733.

Morel, A. (1980). In-water and remote measurements of Ocean color. *Boundary Layer Meteorology*, *18*, 177–201.

Morel, A., et al. (2007). Examining the consistency of products derived from various ocean color sensors in open ocean (Case 1) waters in the perspective of a multi-sensor approach. *Remote Sensing of Environment*, *111*, 69–88.

Morel, A., & Mueller, J. L. (2002). Normalized water-leaving radiance and remote sensing reflectance: Bidirectional reflectance and other factors. In J. L. Mueller (Ed.), *Ocean Optics Protocols For Satellite Ocean Color Sensor Validation, Revision 4, Volume III* (pp. 32–59). Greenbelt: NASA Goddard Space Flight Space Center.

Morel, A., & Prieur, L. (1977). Analysis of variations in ocean color. *Limnology and Oceanography*, *22*, 709–722.

Mueller, J. L., & Morel, A. (2002). *Fundamental Definitions, Relationships and Conventions* 56 pp., Greenbelt.

Park, Y. -J., & Ruddick, K. G. (2005). Model of remote-sensing reflectance including bidirectional effects for case 1 and case 2 waters. *Applied Optics*, *44*, 1236–1249.

Prasad, K. S., et al. (1998). Ocean color algorithms for estimating water clarity (Secchi depth) from SeaWiFS. *Journal of Advanced Marine Science and Technology Society*, *4*, 301–306.

Preisendorfer, R. W. (1986). Secchi disk science: Visual optics of natural waters. *Limnology and Oceanography*, *31*, 909–926.

Roesler, C. S., & Perry, M. J. (1995). In situ phytoplankton absorption, fluorescence emission, and particulate backscattering spectra determined from reflectance. *Journal of Geophysical Research*, *100*, 13279–13294.

Ruddick, K. G., et al. (2000). Atmospheric correction of SeaWiFS imagery for turbid coastal and inland waters. *Applied Optics*, *39*, 897–912.

Simonot, J. -Y., & Le Treut, H. (1986). A climatological field of mean optical properties of the world ocean. *Journal of Geophysical Research*, *91*, 6642–6646.

Stumpf, R. P., et al. (2003). A partially coupled ocean-atmosphere model for retrieval of water-leaving radiance from SeaWiFS in coastal waters, Chap. 9. In S. B. Hooker, & E. R. Firestone (Eds.), *NASA/TM-2003-206892* (pp. 51–59). Greenbelt, MD.

Tyler, J. E. (1968). The Secchi disc. *Limnology and Oceanography*, *13*, 1–6.

Whitmire, A. L., et al. (2007). Spectral variability of the particulate backscattering ratio. *Optics Express*, *15*, 7019–7031.

Zibordi, G., et al. (2006). Comparison of SeaWiFS, MODIS and MERIS radiometric products at a coastal site. *Geophysical Research Letters*, *33*, L06617.